PEOPLE'S DEMOCRATIC REPUBLIC OF ALGERIA

وزارة التعليم العالي والبحث العلمي

Ministry of Higher Education and Scientific Research

جامعة محمد البشير الإبراهيمي– برج بوعريريج –

Mohamed El-Bachir El-Ibrahimi University - Bordj Bou Arreridj

Faculty of Science and Technology

Department of environmental engineering

Thesis

Presented for the award of the **MASTER'S DEGREE**

Field : Process Engineering

Speciality : *Environmental Process Engineering*

By : - Chouder Afaf

- Yousfi Lina Rihab

Subject

Pressure effect on structural, mechanical and electronic properties of SrSe

Defended publicly, on **23/ 06/ 2026**, before the jury composed of:

Mr. Salah Bahah	MCA	**Univ-BBA**	President
Mr. Salah Daoud	Prof	**Univ-BBA**	Examiner
Mr. Ammar Benamrani	MCA	**Univ-BBA**	Supervisor
Mr. Abdelfateh Benmakhlouf	MCA	**Univ-BBA**	Co-Supervisor

Academic Year 2025/2026

Acknowledgments

First and foremost, our deep thanks and praise is to "Allah",

for granting us the opportunity, strength and patience to complete this modest research work.

We would like to extend our sincere thanks and appreciation to all the persons who participated in lighting our path with luminous knowledge candles along our university career,

those who helped us and supported us to be here;

and precisely those who encouraged us along the process of hard working and searching.

With biggest and deepest appreciation, we would like to thank our supervisors Mr. **"Benamrani Ammar "** and Mr. **"Benmakhlouf Abdelfateh "** for their valuable guidance and insightful suggestions and encouragement.

It was a privilege to achieve this manuscript under their supervisions.

We would like to express our warmest thanks to our beloved parents for their great encouragement.

With great respect, besides our supervisor we would like to acknowledge the members of Jury for giving their time to read and correct our work.

And finally,

thanks to all the educational and administrative team of "**Mohamed El-Bachir El-Ibrahimi University - Bordj Bou Arreridj –**".

Dedication

With deep gratitude to Allah the almighty for his blessings, I extend my heartfelt thanks to those who have been my guiding lights and pillars of support throughout this research. To the one who always pushed me forward towards my goals and to the one who dedicated himself to my education with immense sacrifices, revering knowledge: my dear father, may his days be long. To the one who gave her all in love and care, who endured everything, who was my rock in times of hardship: my mother, the dearest angel to my heart and eyes.

To them, I dedicate this humble work, which brings some happiness to their hearts.

To my siblings: ***Haroun, Sara*** *and* ***Yasmine***

To my supervisors: Benamrani Ammar and Benmakhlouf Abdelfateh.

To my dear family.

To my lifelong friend and my partner in this work: ***Lina Rihab****, This is not our first achievement together, and I hope it will not be the last. I am grateful for every challenge, success, and unforgettable moment we experienced together.*

To and to all who supported me, even with a word, I send my appreciation to you all. Your kindness band support means the world to me.

AFAF

Dedication

Praise be to God, and thanks to God first for completing this work.

Every challenging work needs self-efforts as well as guidance of elders especially those who are very close to our heart.

I dedicate my humble effort to my dear

Father and Mother

Whose affection, love, encouragement and prays of days and night makes me able to get such success and honor.

*To my siblings: "**Yahia, Idris, Intissar**," who have never left my side just wanted to say that I really appreciate this.*

*To my friend of my life, who is the companion of my path and the smile of my heart, she is the partner of my memories. God will never separate us **Afaf** thanks for her for sharing with me the difficulties of this manuscript.*

To everyone who helped me in this work, from near or far.

This humble work is a sign of my love to you.

Lina

Abstract

Due to their use in electrical and optoelectronic devices, semiconductor materials are crucial to contemporary technologies. Due to their intriguing physical characteristics, II–VI compound semiconductors have garnered a lot of attention. This work uses first-principles calculations based on Density Functional Theory (DFT) to study the structural, electrical, mechanical, and thermodynamic properties of strontium selenide (SrSe) semiconductor in the NaCl-type structure. The plane-wave pseudopotential approach's CASTEP code was used for the computations. Analysis was done on the thermodynamic characteristics, mechanical behavior, elastic properties, and structural stability. Additionally, the band structure and density of states computations were used to examine the electronic properties.

The results obtained shed light on the physical characteristics of SrSe and demonstrate its potential as a promising material for optoelectronic and semiconductor applications.

Keywords: SrSe, II–VI semiconductors, Density Functional Theory, CASTEP, structural properties, mechanical properties, thermodynamic properties.

Résumé

En raison de leur utilisation dans les dispositifs électriques et optoélectroniques, les matériaux semi-conducteurs jouent un rôle crucial dans les technologies contemporaines. De par leurs caractéristiques physiques fascinantes, les semi-conducteurs composés II-VI ont suscité un vif intérêt. Ce travail utilise des calculs de première principe basés sur la théorie de la fonctionnelle de la densité (DFT) pour étudier les propriétés structurales, électriques, mécaniques et thermodynamiques du semi-conducteur à base de séléniure de strontium (SrSe) présentant une structure de type NaCl.

Le code CASTEP, basé sur l'approche du pseudopotentiel à ondes planes, a été utilisé pour les calculs. L'analyse a porté sur les caractéristiques thermodynamiques, le comportement mécanique, les propriétés élastiques et la stabilité structurelle. De plus, des calculs de la structure de bande et de la densité d'états ont été effectués afin d'étudier les propriétés électroniques.

Les résultats obtenus apportent un éclairage sur les caractéristiques physiques du SrSe et démontrent son potentiel en tant que matériau prometteur pour des applications optoélectroniques et dans le domaine des semi-conducteurs.

Mots-clés : SrSe, semi-conducteurs II-VI, théorie de la fonctionnelle de la densité, CASTEP, propriétés structurales, propriétés mécaniques, propriétés thermodynamiques.

ملخص

تُعد مواد أشباه الموصلات ذات أهمية بالغة للتقنيات المعاصرة، وذلك بسبب استخدامها في الأجهزة الكهربائية والضوئية. .وقد حظيت أشباه الموصلات المركبة من الفئة II–VI باهتمام كبير بفضل خصائصها الفيزيائية المثيرة للاهتمام. يستخدم هذا العمل حسابات المبادئ الأولى المستندة إلى نظرية وظيفية الكثافة (DFT) لدراسة الخصائص الهيكلية والكهربائية والميكانيكية والحرارية لأشباه الموصلات من سيلينيد السترونتيوم (SrSe) ذات البنية من نوع NaCl.

وقد استُخدم برنامج CASTEP القائم على نهج الجهد الزائف للموجة المستوية لإجراء الحسابات. وأُجري تحليل للخصائص الديناميكية الحرارية، والسلوك الميكانيكي، والخصائص المرنة، والاستقرار الهيكلي. بالإضافة إلى ذلك، استُخدمت حسابات بنية النطاق وكثافة الحالات لدراسة الخصائص الإلكترونية.

تسلط النتائج التي تم التوصل إليها الضوء على الخصائص الفيزيائية لمركب SrSe وتُظهر إمكاناته كمواد واعدة في تطبيقات الإلكترونيات الضوئية وأشباه الموصلات.

الكلمات المفتاحية: SrSe، أشباه الموصلات من المجموعة II–VI، نظرية وظيفية الكثافة، CASTEP، الخصائص الهيكلية، الخصائص الميكانيكية، الخصائص الديناميكية الحرارية.

Table of Contents

General Introduction 1

References 3

PART ONE: BIBLIOGRAPHIC STUDY

Chapter I: **Semiconductors**

I.1 Introduction 6

I.2 Fundamentals of Semiconductors 8

I.2.1 Atomic Energy Level Splitting and Band Formation 8

I.2.2 Doped Semiconductors: N-type and P-type Materials 8

I.2.3 Semiconductor Charge Carriers 10

I.2.4 Intrinsic and Extrinsic Semiconductors: Electronic Behaviors 10

I.3 Electronic Properties and Band Structures of Semiconductors: 11

I.3.1 Electronic Energy Band Structure Principles 11

I.3.2 Energy Gap 12

I.4 Binary Semiconductors 14

I.4.1 III–V Semiconductors 15

I.4.2 II–VI Semiconductors 16

I.5 Overview of Strontium Selenide (SrSe) 16

I.5.1 Introduction to Strontium Selenide: 16

I.5.2 Crystal structure of SrSe 17

I.5.3 Electronic properties of SrSe 17

I.5.4 Applications of SrSe 17

I.5.5 Importance of theoretical studies on SrSe 18

References 19

Chapter II: Quantum methods and simulation code

II.1. Introduction 23

II.2 Methods of quantum chemistry 23

II.2.1 Equation de Schrödinger 23
II.3. Basic approximations 24
II.3.1. Born–Oppenheimer Approximation 24
II.3.2 Hartree-Fock approximation 26
II.3.3. Hartree-Fock-Roothan method 27
II.3.4 Density Functional Theory (DFT) 27
II.3 Simulation code : (CASTEP programme) 34
II.3.1 Definition 34
II.3.2. Background theory 35
II.3.3 CASTEP capabilities 36
II.3.4. Future development 37
II.3.5. Availability 37
References 38

PART TWO: PRACTICAL STUDY

Chapter III: Results and Interpretations

III.1 Introduction 44
III.2 Computational Method 44
III.3 Structural Properties 45
III.3.1 Crystal Structure 45
III.3.2 Energy-Volume Equation of State (EOS) 46
III.3.3 Analysis and Structural Discussion 47
III.3.4 Evaluation of Crystalline Density under Hydrostatic Pressure 47
III.3.5 Density Variation Analysis 48
III.4 Mechanical Stability and Elastic Responses 49
III.4.1 Fundamental Cubic Elastic Constants (Cij) Definitions 49
III.4.2 Criteria for Mechanical Stability 51
III.4.3 Acoustic Elastic Wave Velocities and Debye Temperature 52
III.5 Electronic Properties 55

III.5.1 Energy Band Structures under Pressure 55
III.5.2 Pressure Dependence of the Energy Band Gap 56
III.5.3 Density of States (DOS) Analysis 57
III.6 Conclusion 58
References 60
General conclusion 62

List of Figures

Figure I. 1 Energy band diagram: Insulator, Semiconductor and Metal 6
Figure I. 2 N-Type Semiconductors 9
Figure I. 3 P-Type Semiconductors 9
Figure I. 4 Intrinsic Semiconductor 10
Figure I. 5. Representation of the conduction and valence bands 12
Figure I. 6. Representation of the direct band gap 13
Figure I. 7. Representation of the indirect band gap 13
Figure I. 8 Stripe geometry laser in which the oxide layer isolates all but the stripe contact 14

Figure II. 1. Implementation of the Born-Oppenheimer approximation algorithm 25
Figure II. 2. Flowchart illustrating the method for solving the Kohn–Sham equation 33

Figure III. 1 3D unit cell structure of SrSe compound. 45
Figure III. 2 Fitted E-V data for SrSe compound 46
Figure III. 3 Variation of crystalline density and unit volume with pressure of SrSe compound 48
Figure III. 4 Elastic constants of SrSe compound as a function of pressure. 50
Figure III. 5 Mechanical stability criterion of SrSe compound as a function of pressure 52
Figure III. 6: Variation of sound velocities of SrSe compound as a function of pressure 54
Figure III. 7 Debye temperature of the studied SrSe. 55
Figure III. 8 Band structures of SrSe at different pressures 56
Figure III. 9 Variation of SrSe band gap with pressure 57
Figure III. 10 : Density of States of SrSe compound. 58

List of Tables

Table I. 1 Properties of some common semiconductors …….. 15

Table II. 1 Correspondence between structural or external perturbations and their derived second-order physical quantities. 35

Table III. 1 Structural parameters of SrSe compound.....46
Table III. 2 Analytical fitting equations for the pressure dependence of normalized volume (V/V0) and crystalline density (d) of SrSe compound using GGA approximation.....48
Table III. 3 Elastic constants of SrSe compound at zero pressure ($\boldsymbol{P = 0\ GPa}$) 49
Table III. 4 Calculated polycrystalline bulk modulus (K), shear modulus (G), and shear parameter (G') (in GPa) of SrSe compound under different hydrostatic pressures.....51
Table III. 5 Calculated longitudinal (vl), transverse (vt), and average (vm) acoustic velocities (in m/s) of SrSe compound under high pressure. 53
Table III. 6 Pressure evolution of the calculated direct energy band gap Eg (in eV) for SrSe compound. 56

List of Abbreviations

Al : Aluminum

Ag : Silver

Au : Gold

B : Bulk modulus

CASTEP : Cambridge Sequential Total Energy Package

Co-ord. No.: Coordination Number

Cu : Copper

DFT : Density Functional Theory

DFPT : Density Functional Perturbation Theory

DOS : Density of States

Eg : Energy Band Gap

EOS : Equation of State

eV : Electron-volt

fcc : Face-centered cubic

Fe : Iron

GGA : Generalized Gradient Approximation

GPa : Gigapascal

IR : Infrared

KS : Kohn-Sham

LDA : Local Density Approximation

LEDs : Light-Emitting Diodes

LO/TO : Longitudinal Optical / Transverse Optical

LST/QST : Linear Synchronous Transit / Quadratic Synchronous Transit

LYP : Lee, Yang, and Parr functional

MD : Molecular Dynamics

MO: Molecular orbitals

AO : Atomic orbitals

NaCl : Sodium Chloride phase

PBE : Perdew-Burke-Ernzerhof functional

PW91 : Perdew and Wang functional

RPBE : Revised Perdew-Burke-Ernzerhof functional

SiO_2 : Silicon dioxide

SrSe : Strontium Selenide

WDA : Weighted Density Approximation

Z : Number of formula units per unit cell

General Introduction

The continuous development of modern technologies has created an increasing demand for advanced materials with specific physical properties. Among these materials, semiconductor compounds occupy a significant position due to their unique electrical and optical characteristics, which make them essential for various applications such as electronic devices, optoelectronic systems, photovoltaic cells, and radiation detection technologies [1,2].

Among semiconductor materials, II–VI compounds have attracted considerable attention because of their interesting electronic structures and suitable band gap energies. These materials offer important advantages for technological applications, particularly in light emission, photodetection, and energy conversion devices [3,4,5].

Strontium selenide (SrSe) is a binary II–VI semiconductor composed of strontium and selenium. Due to its interesting structural and electronic properties, SrSe has been investigated as a promising material for different applications, especially when its physical properties are properly understood and optimized [6,7]. Therefore, studying its fundamental properties is essential for evaluating its potential in semiconductor technologies.

The investigation of materials properties requires accurate theoretical approaches. In this context, first-principles calculations based on Density Functional Theory (DFT) have become powerful tools for predicting the structural, electronic, mechanical, and thermodynamic properties of materials without requiring experimental parameters. The development of DFT by Hohenberg and Kohn, followed by the Kohn–Sham formulation, has provided an efficient framework for studying complex electronic systems [8, 9].

In this work, first-principles calculations are performed to investigate the physical properties of SrSe semiconductor. The study focuses on structural optimization, electronic structure, mechanical behavior, and thermodynamic properties using the CASTEP simulation code within the framework of Density Functional Theory.

This thesis is organized into three main parts:

The first chapter presents a general overview of semiconductor materials. It introduces the basic concepts of semiconductors, their classification, characteristics, and applications. Particular attention is given to II–VI semiconductor compounds and the structural and physical properties of SrSe.

The second chapter is devoted to the theoretical methods used in this work. It describes the fundamental concepts of quantum calculations, the Schrödinger equation, different approximations, and especially Density Functional Theory with the Hohenberg–Kohn and Kohn–Sham approaches. The exchange-correlation approximations and the CASTEP simulation code are also presented.

The third chapter presents the computational details and discusses the obtained results. The structural, electronic, mechanical, and thermodynamic properties of SrSe are analyzed and interpreted in order to understand its physical behavior and evaluate its potential applications.

References

[1] H,Yahi. Physique des semi-conducteurs. Université 8 Mai 1945 Guelma, 2020/2021.

Link: https://dspace.univ-guelma.dz/jspui/handle/123456789/12500

[2] B.G. Yacobi, Semiconductor Materials: An Introduction to Basic Principles, Springer 2003 ISBN 0306473615, pp. 1–3.

[3] S. Adachi, Properties of Group-IV, III-V and II-VI Semiconductors, Wiley, 2005.

[4] A. Rockett, The Materials Science of Semiconductors, Springer, 2008.

[**5**] S. M. Sze and K. K. Ng, *Physics of Semiconductor Devices*, 3rd ed., Wiley, 2007.

[6] Labidi, S., Meradji, H., Slimani, M., Ghemid, S., El Haj Hassan, F., & Bouhafs, B.,"First principles calculations of structural, electronic and thermodynamic properties of SrS, SrSe, SrTe compounds and $SrS_{1-x}Se_x$ alloy", *Physics Procedia, 2*, 1009–1016 (2009).

[7] H. M. Crosswhite et al., "Crystal structure and electronic properties of SrSe compounds," Journal of Applied Physics.

[8] P. Hohenberg and W. Kohn, "Inhomogeneous Electron Gas," Physical Review, 136, B864 (1964).

[9] W. Kohn and L. J. Sham, "Self-consistent equations including exchange and correlation effects," Physical Review, 140, A1133 (1965).

PART ONE: BIBLIOGRAPHIC STUDY

Chapter I: Semiconductors

I.1 Introduction

Materials are classified into three categories according to their electrical properties: conductors, insulators, and semiconductors **(Figure I.1).**

Conductors are metals such as iron (Fe), copper (Cu), gold (Au), silver (Ag), and aluminum (Al). They have the lowest resistivity at room temperature, typically less than 10^{-5} Ω.cm. Electrical conduction in these metals occurs primarily through free electrons located in the outer shells of their constituent atoms.

On the other hand, insulators are materials with a very high resistivity ($\rho > 10^{8}$ Ω.cm), such as glass, mica, silica (SiO_2), and diamond. In these materials, electrons are tightly bound to their atoms, which make the flow of electric current extremely difficult [1].

Between these two extremes are semiconductors, which possess a crystalline structure and contain very few free electrons at room temperature. As a result, they behave almost like an insulator, and their resistivity lies between that of conductors and insulators. However, by adding suitable impurities, their conductivity can be controlled. Examples of semiconductors include silicon, germanium, and diamond.

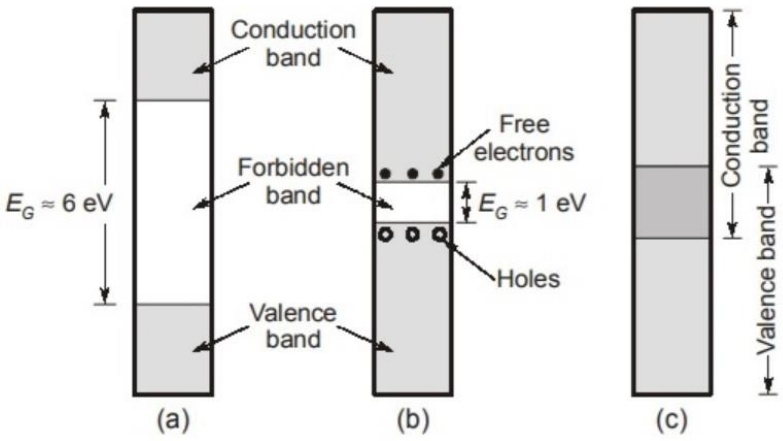


Figure I. 1 Energy band diagram: Insulator, Semiconductor and Metal [2]

Semiconductors are the basic building block of modern electronics, including transistors, solar cells, light-emitting diodes (LEDs), and digital and analog integrated circuits. The modern understanding of the properties of a semiconductor lies on quantum physics to explain the

movement of electrons and holes inside a crystal structure and also in a lattice. An increased knowledge of semiconductor materials and fabrication processes has made possible continuing increases in the complexity and speed of microprocessors.

The electrical conductivity of a semiconductor material increases with increasing temperature, which is behavior opposite to that of a metal. Semiconductor devices can display a range of useful properties such as passing current more easily in one direction than the other, showing variable resistance, and sensitivity to light or heat. Because the electrical properties of a semiconductor material can be modified by controlled addition of impurities or by the application of electrical fields or light, devices made from semiconductors can be used for amplification, switching, and energy conversion. Current conduction in a semiconductor occurs through the movement of free electrons and "holes", collectively known as charge carriers.

Development of quantum physics in turn allowed the development of the transistor in 1948. Although some pure elements and many compounds display semiconductor properties, silicon, germanium, and compounds of gallium are the most widely used in electronic devices. A large number of elements and compounds have semiconducting properties, including [2], certain pure elements are found in Group XIV of the periodic table; the most commercially important of these elements are silicon and germanium. Silicon and germanium are used here effectively because they have 4 valence electrons in their outermost shell which gives them the ability to gain or lose electrons equally at the same time.

Binary compounds, particularly between elements in groups III and V, such as gallium arsenide, groups II and VI, groups IV and VI, and between different group IV elements, e.g. silicon carbide. Certain ternary compounds, oxides and alloys. Organic semiconductors, made of organic compounds. Most common semiconducting materials are crystalline solids, but amorphous and liquid semiconductors are also known. These include hydrogenated amorphous silicon and mixtures of arsenic, selenium and tellurium in a variety of proportions. These compounds share with better known semiconductors the properties of intermediate conductivity and a rapid variation of conductivity with temperature, as well as occasional negative resistance. Such disordered materials lack the rigid crystalline structure of conventional semiconductors such as silicon. They are generally used in thin film structures, which do not require material of higher electronic quality, being relatively insensitive to impurities and radiation damage. Now-a-days semiconductor materials are used in every sector of modern technology. In technical purpose the high temperature materials are used widely. Therefore, it is needed to increase the

temperature of semiconducting materials. For these reasons, the different properties of these materials varied with temperature. In this paper we review the classification of semiconductors, early history of semiconductors and temperature effects in semiconductors [3].

I.2 Fundamentals of Semiconductors

I.2.1 Atomic Energy Level Splitting and Band Formation

The fundamental difference between semiconductors and other materials lies in their distinct band structures. The core of electronic properties is band theory. The key to band theory is energy level splitting. Due to the Pauli exclusion principle [4], in crystal structures, no two electrons can simultaneously occupy the same quantum state. Energy level splitting in crystal structures occurs at their corresponding characteristic atomic spacing. Because of the physical constraint of repulsive forces between different types of atoms, atomic boundaries are established. These atomic constraints set clear limits on the degree of energy level splitting, resulting in different energy bands. Each energy level comprises multiple closely spaced states. Electrons move freely within these energy bands, and the electronic behavior of these bands fundamentally determines whether a material's electronic properties are those of an insulator, conductor, or semiconductor [5].

I.2.2 Doped Semiconductors: N-type and P-type Materials

Pure intrinsic semiconductor materials have an extremely limited application in electronic device manufacturing due to their low electrical conductivity at room temperature. By introducing specific impurity atoms into the pure semiconductor matrix—a process known as **doping**—the conductivity of the material can be precisely controlled. This enhancement in conductivity primarily results from the significant modification of free electron and hole densities within the crystal lattice. Doped semiconductors are generally classified into two main types: N-type and P-type materials.

I.2.2.1 N-type semiconductors

In N-type semiconductors, electrons serve as the majority charge carriers, while holes represent the minority carriers. For a semiconductor composed of Group XIV elements, such as Silicon (Si), the doping impurities are selected from Group XV (e.g., Phosphorus, P). Because Group XV atoms possess five valence electrons—one more than Silicon—they provide an extra free electron to the conduction band, acting as **donor atoms**. The energy required to detach this extra

electron from its parent atom is significantly lower than that needed to break a standard covalent bond, thereby remarkably increasing the material's conductivity.

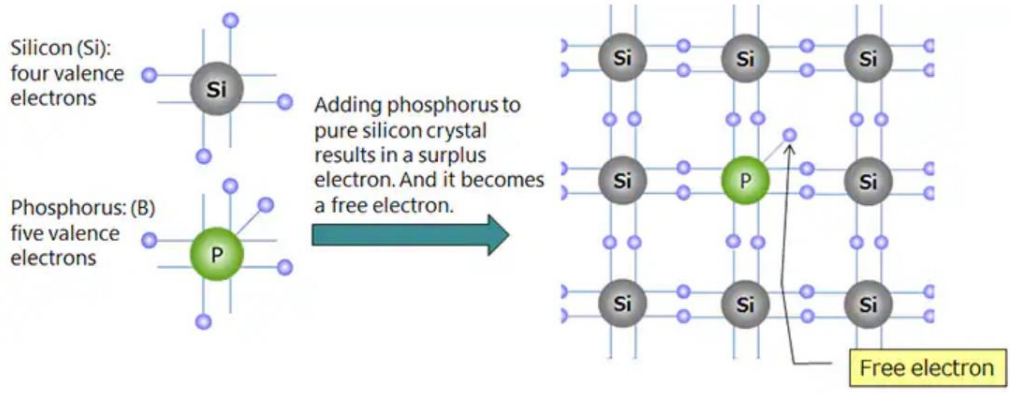


Figure I. 2 N-Type Semiconductors [7]

I.2.2.1 P-type semiconductors

In P-type semiconductors, holes act as the majority charge carriers and electrons become the minority carriers. In this case, the semiconductor is doped with Group XIII elements (e.g., Boron, B), which are termed **acceptor atoms**. Since Boron has only three valence electrons (one less than Silicon), it creates an electron deficiency or a "hole" in the valence band [5]. This generated hole can easily accept a valence electron from a neighboring Silicon atom, facilitating electrical conduction through whole movement, as illustrated in Figure I.3.

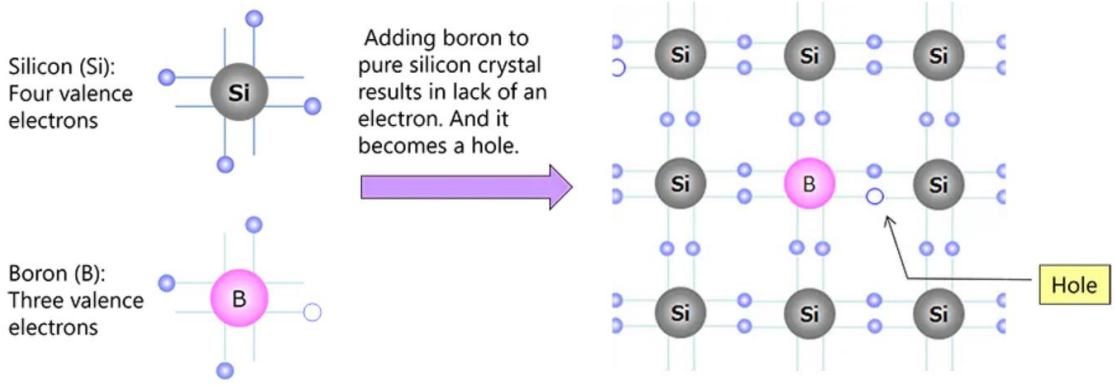


Figure I. 3 P-Type Semiconductors [7]

I.2.3 Semiconductor Charge Carriers

Semiconductors are solid materials intermediate between metals and insulators, generated by electronic particles (electrons or holes). Charge carriers are generated through intrinsic excitation (thermal excitation), doping introduction, and the generation of charge carriers. Current is primarily due to various scattering mechanisms of conduction electrons, such as lattice vibrations, impurities, lattice defects, grain boundaries, and vacancies. For example, excessively high doping concentrations can increase ion hybridization scattering and reduce migration rates. Simultaneously, external conditions such as temperature, electric field strength, and strain stress also affect charge carrier transport [5].

I.2.4 Intrinsic and Extrinsic Semiconductors: Electronic Behaviors

I.2.4.1 Intrinsic Semiconductor

An intrinsic semiconductor is a semiconductor that has not been intentionally doped with impurities. These semiconductors are extremely pure and possess a highly ordered crystal structure, with a perfectly periodic lattice. Moreover, their impurity level is very low, with less than one impurity atom per 10^{13} atoms of the semiconductor element. This ensures that the electrical properties of the intrinsic material are primarily determined by its crystal structure and the characteristics of the electrons in its valence band and conduction band. Intrinsic semiconductors are used as a reference to study the fundamental properties of semiconductors and to evaluate the effect of dopants on their conductivity and electronic properties [6].

Figure I.4 provides a general overview of intrinsic semiconductors in terms of band structure and charge carrier distribution.

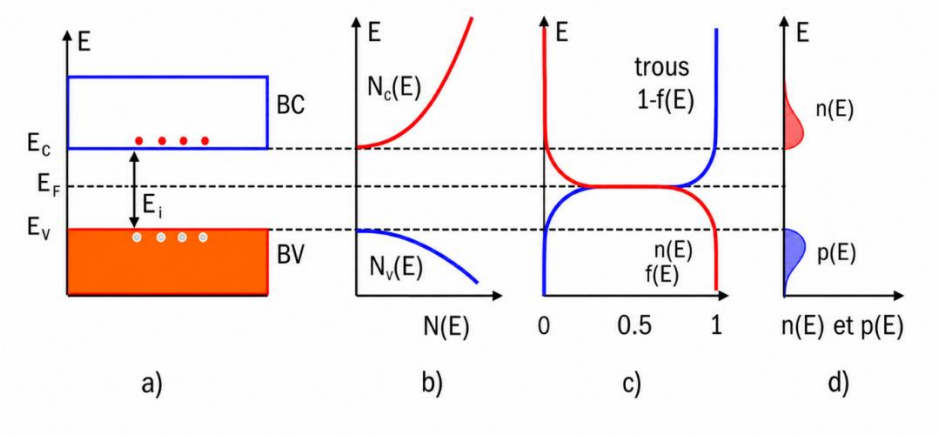


Figure I. 4 Intrinsic Semiconductor [9]

a) Energy Band Diagram

b) Energy Density of States

c) Fermi-Dirac Distributions

d) Energy Distributions of Carriers (n and p carrier densities correspond to the shaded areas)

I.2.4.2 Extrinsic Semiconductor

In intrinsic or pure semiconductors, the concentration of electrons and holes at normal temperatures is very low. As a result, to achieve a noticeable current density through the semiconductor, a strong electric field must be applied.

This limitation can be overcome by introducing suitable impurities into intrinsic semiconductors. Extrinsic semiconductors are those in which a significant amount of impurities is present [6]. In general, the impurities can be elements from either group III or group V of the periodic table. Based on the type of impurity added, extrinsic semiconductors are classified into two categories: n-type semiconductors and p-type semiconductors [7].

I.3 Electronic Properties and Band Structures of Semiconductors:

The electronic properties of semiconductor materials are fundamentally dictated by their underlying band structures, where the width of the forbidden energy band gap (Eg) defines their intrinsic level of electrical conductivity. Over the decades, considerable theoretical and experimental efforts have been made to accurately determine the band structures of various semiconductors. These extensive studies aim to map the precise energy levels of electrons and holes within the valence and conduction bands, thereby allowing researchers to assess transport properties and specific electronic characteristics. However, determining the exact band structure remains an extremely complex challenge, primarily due to the lack of a direct analytical expression for the crystal's periodic potential energy.

I.3.1 Electronic Energy Band Structure Principles

Electronic energy band structures indicate the allowed quantum energy states for electrons plotted as a function of their wave vector (K). Consequently, these bands are mathematically represented in the reciprocal space (or K-space) and, for simplicity, are mapped along the directions of the highest symmetry within the first Brillouin zone.

These energy states are broadly divided into valence bands and conduction bands. Specifically, it is the highest valence band, the lowest conduction band, and the forbidden band gap (Eg) that separates them, which primarily determine the electronic and charge transport properties of the semiconductor.

At absolute zero temperature (T = 0 K), the valence band is completely filled with electrons in a perfect, intrinsic semiconductor. Structurally, for conventional diamond or zinc-blende crystals, the atomic orbitals hybridize to form bonding and antibonding states. The bonding configurations form the filled valence bands, while the remaining four antibonding orbitals give rise to the upper bands that form the conduction band, which remains entirely empty at 0 K.

Depending on the coordinate positions of these band extrema in the reciprocal space, semiconductors are classified into direct and indirect types. In direct band gap semiconductors, the maximum of the valence band and the minimum of the conduction band are perfectly aligned at the exact same wave vector, which is typically located at the Γ point [8]. This alignment allows for efficient, direct photon emission and absorption, which is the key for optoelectronic devices.

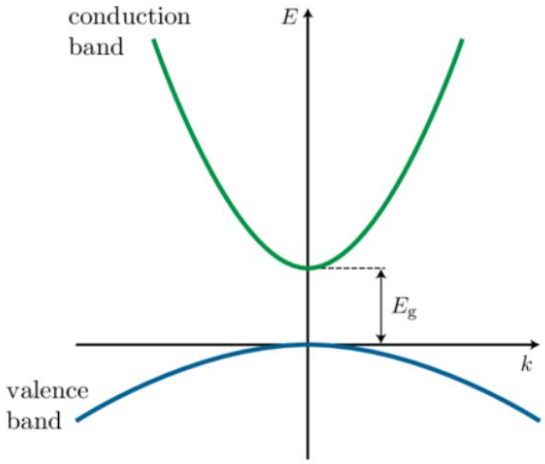


Figure I. 5. Representation of the conduction and valence bands [12]

I.3.2 Energy Gap

The gap is by definition the width of the band gap, that is, the energy difference between the absolute minimum of the conduction band and the absolute maximum of the valence band.

Therefore, there are two fundamental types of semiconductors: direct gap semiconductors and indirect gap semiconductors [8].

I.3.2.1 Direct Band Gap:

A semiconductor is a direct band gap semiconductor if the valence band maximum and the conduction band minimum correspond to the same wave vector K. (The central conduction band minimum corresponds to electrons with low effective mass, and therefore very mobile) [9].

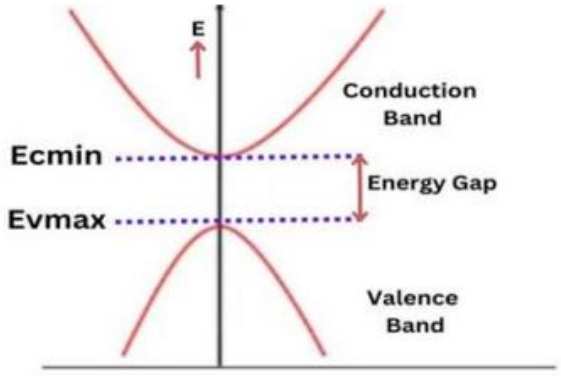


Figure I. 6. Representation of the direct band gap [14]

I.3.2.2 Indirect Band Gap

Indirect gap semiconductors, in which the minimum of the conduction band and the maximum of the valence band are located at different points in k-space (their conduction band corresponds to electrons with a high effective mass, and therefore low mobility) [9].

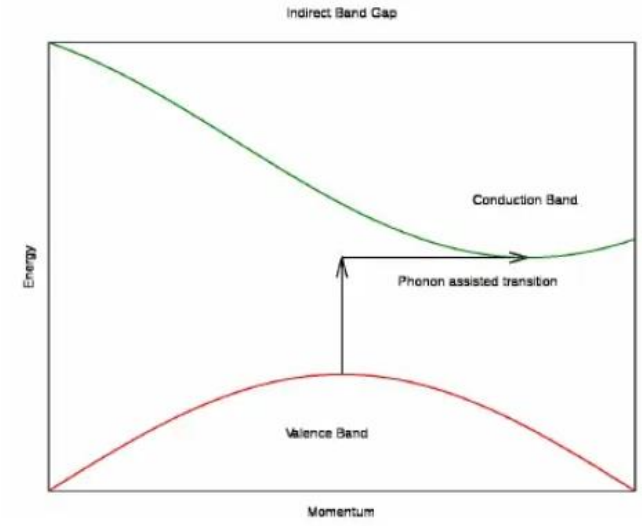


Figure I. 7. Representation of the indirect band gap [16]

I.4 Binary Semiconductors

Important semiconducting materials include the III–V (13–15) materials such as GaAs or InP, and II–VI (12–16) materials such as CdS or ZnSe (Table 1). These compound semiconductors are most often formed by combining elements displaced on either side of silicon by one place (i.e., III ¼ Ga or In and V ¼ N or As for a III–V material) or two places (i.e., II ¼ Zn or Cd and VI ¼ S or Se for a II–VI material) in the periodic table. Other materials are of specialist importance, especially ternary materials such as CuInE2 (E ¼ S and Se), which find applications in solar cell technologies, as do materials of III–VI composition such as InxSy, although their properties are often complicated by the potential for the formation of a wide range of similar phases.

One important feature of compound semiconductors is that their bands span a much wider range that of elemental silicon and can therefore cover a wider range of the electromagnetic spectrum, in particular the visible region. Compound semiconductors are also more often ‘‘direct,’’ i.e., there is conservation of the wave vector for optical transitions, leading to allowed transitions with large absorption coefficients [10].

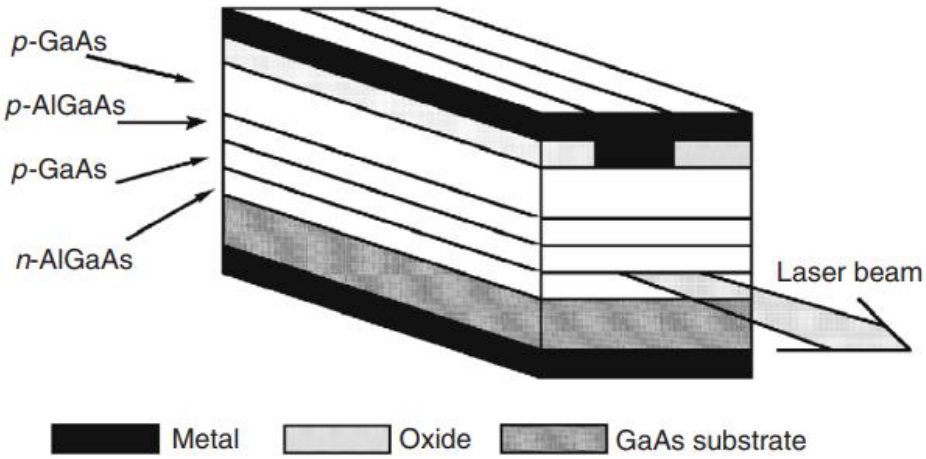


Figure I. 8 Stripe geometry laser in which the oxide layer isolates all but the stripe contact (stripe widths are usually in the region of 3–30 mm).

Table I. 1 Properties of some common semiconductors [17]

Compound	*Band gap*[a] (eV)	*Type*[b]	*Structure*	*Lattice spacing* (Å)	*Applications*
Si	1.11	i	Diamond	5.43	Integrated circuits, power electronics
Ge	0.67	i	Diamond	5.66	
III–V materials					
GaP	2.25	i	Zinc blende	5.450	LED
GaAs	1.43	d	Zinc blende	5.653	High-speed integrated circuits, displays
GaSb	0.69	d		6.095	Thermal imaging devices
InP	1.28	d	Zinc blende	5.8687	Transistor devices
InAs	0.36	d	Zinc blende	6.058	
InSb	0.17	d		6.4787	
II–VI materials					
CdS	2.53	d	Wurtzite	*a*: 4.136; *c*: 6.713	Photovoltaic cells
CdSe	1.74	d	Wurtzite	*a*: 4.299; *c*: 7.010	Photovoltaic cells
CdTe	1.50	d	Zinc blende	6.477	Photovoltaic cells, electrooptic modulators
ZnS	3.8	d	Wurtzite	*a*: 3.814; *c*: 6.257	Phosphors, infrared windows
ZnS	3.6	d	Zinc blende	5.406	
ZnSe	2.58	d	Zinc blende	5.667	Infrared windows, LEDs
ZnTe	2.28	d	Zinc blende	6.101	
IV–VI materials					
PbS	0.37	d	NaCl	5.936	Infrared sensors
PbSe	0.26	d	NaCl	6.124	Infrared sensors
PbTe	0.29	d	NaCl	6.460	Infrared sensors

[a] At 300 K. [b] d, direct; i, indirect.

I.4.1 III–V Semiconductors

The applications of III–V materials represent a fairly well-developed area of technology. Most applications of such semiconductors are in the area of optoelectronics; there are many commercial processes for the manufacture of light-emitting diodes (LEDs) and solid-state lasers.3 Gallium arsenide solar cells are commonly used to power satellites. Development of LED and laser technologies for the blue end of the electromagnetic spectrum using gallium nitride is in progress at a number of research institutes and commercial corporations. The majority of III–V materials are direct bandgap materials; switching in these is faster than in indirect materials such as silicon. Complete device technologies based on direct bandgap materials has led to the production of devices faster than the equivalent ones fabricated from silicon—such as is needed in many wireless devices and applications [10].

I.4.2 II–VI Semiconductors

The wide-bandgap, direct-transition nature of II–VI materials is similar to that of the III–V materials, but the bandgap energies are in general larger and more suited to applications in optical and optoelectronic devices. II–VI compounds have generally been limited to simple applications as in optical coatings, gratings, or photoconductors. However, heteroepitaxial technologies have started to be developed and advances in chemical vapor deposition (CVD) techniques may open up new device fabrication methods for new applications. The principal II–VI compounds have structures closely related to that of ZnS and there is the possibility of growing both cubic and hexagonal phases during the deposition of thin layers. II–VI compounds are potentially important materials for the emission, detection, and modulation of light in the visible and near-UV region [11-12].

Among the various promising members of the II–VI family, alkaline-earth chalcogenides, and specifically **Strontium Selenide (SrSe)**, have attracted considerable attention due to their distinct structural stability and wide electronic bandgap. Therefore, this study is devoted to investigate the physical properties of this specific compound, beginning with a detailed overview of its fundamental parameters.

I.5 Overview of Strontium Selenide (SrSe)

I.5.1 Introduction to Strontium Selenide:

Strontium selenide (SrSe) is a binary semiconductor belonging to the II–VI semiconductor family [13,14]. It is composed of strontium (Sr), an alkaline earth metal belonging to group II of the periodic table, and selenium (Se), a chalcogen element belonging to group VI [15].

II–VI semiconductor compounds have attracted considerable attention due to their interesting electronic, optical, mechanical, and thermal properties [14,16]. These materials exhibit a wide range of applications in modern optoelectronic devices, including light-emitting diodes, photovoltaic systems, and radiation detectors [16,17].

SrSe is considered a promising semiconductor material because of its suitable electronic structure, chemical stability, and potential applications in advanced electronic and optical technologies [18].

I.5.2 Crystal structure of SrSe

The physical properties of semiconductor materials are strongly influenced by their crystal structure [15]. SrSe crystallizes mainly in the cubic rock-salt structure (NaCl-type structure), where each strontium atom is surrounded by six selenium atoms and each selenium atom is surrounded by six strontium atoms [18,19].

This arrangement corresponds to a high-symmetry structure belonging to the Fm-3m space group [19].

The lattice parameter, atomic positions, and bonding characteristics of SrSe play an important role in determining its electronic properties, mechanical stability, and thermal behavior [18,20].

The investigation of structural properties is therefore an essential step before studying the other physical characteristics of this compound [21].

I.5.3 Electronic properties of SrSe

The electronic properties of SrSe are related to the interaction between Sr and Se atoms and the distribution of electrons within the crystal lattice [18,22].

As a semiconductor, SrSe possesses an energy band gap separating the valence band and the conduction band. This band gap controls its electrical conductivity and optical response [15,22].

The study of band structure, density of states (DOS), and band gap energy provides important information about the possibility of using SrSe in electronic and optoelectronic applications [22,23].

I.5.4 Applications of SrSe

Due to its interesting physical properties, SrSe and related II–VI semiconductor compounds have been investigated for several technological applications [16,17].

I.5.4.1 Optoelectronic devices

II–VI semiconductors are widely studied for optoelectronic applications because their band gaps can be suitable for light emission and detection processes [16].

I.5.4.2 Phosphors and luminescent materials

Strontium selenide compounds have been investigated as host materials for luminescent applications, especially when doped with rare-earth ions [24].

I.5.4.3 Photovoltaic applications

The electronic and optical characteristics of II–VI compounds make them potential candidates for photovoltaic applications [17].

I.5.4.4 Radiation detection

Semiconductor materials with appropriate electronic structures can be used in radiation detection systems due to their interaction with high-energy photons [25].

I.5.5 Importance of theoretical studies on SrSe

Experimental investigations alone may not provide complete information about the fundamental properties of semiconductor materials. Therefore, theoretical methods such as Density Functional Theory (DFT) have become powerful tools for predicting and analyzing material properties [26, 27].

DFT calculations allow the investigation of structural, electronic, mechanical, and thermal properties without requiring extensive experimental measurements [26].

In this work, first-principles calculations based on Density Functional Theory are performed to study the structural, electronic, mechanical, and thermal properties of SrSe semiconductor.

References

[1] H,Yahi, Physique des semi-conducteurs. Université 8 Mai 1945 Guelma, 2020/2021.

Link: https://dspace.univ-guelma.dz/jspui/handle/123456789/12500

[2] B.G. Yacobi, Semiconductor Materials: An Introduction to Basic Principles, Springer 2003 ISBN 0306473615, pp. 1–3.

[3] M. A. Rahman, "A Review on Semiconductors Including Applications and Temperature Effects in Semiconductors", American Scientific Research Journal for Engineering, Technology, and Sciences (ASRJETS), Vol. 7, pp. 50-70, 2014.

[4] Abushagur, M.A.G. (2025). Semiconductor Energy Bands. In: Applied Photonics. Graduate Texts in Physics.Springer, Cham.https: //doi.org/10.1007/978-3-031-86457-5_10

[5] A. Yakoubi, A. S. Verma, and L. Yakoubi, "Structural, mechanical and thermodynamic properties of SrSe in CsCl phase," Physica B: Condensed Matter, vol. 427, pp. 110-116, 2013.

[6] K. Wahiba, "Doctoral Thesis: Study of Electronic Band Structures and Properties Related to Quasi-binary Semiconductors $(GaP)_{1-x}(ZnSe)_x$", Mohamed Khider University – Biskra, 2011.

[7] B. Mohamed, "Doctoral Thesis: Study of Laser Nanostructures Based on GaNSb/AlGaInNSb Antimonide Nitrides", Djilali Liabes University – Sidi Bel Abbes, 2014.

[8] R. Mendoud, I. Saha, Energy gaps and optical properties for the ternary semiconductor alloys, Master's thesis, Department of Electronics, Faculty of Science and Technology, Mohamed El-Bachir El-Ibrahimi University - Bordj Bou Arreridj, 2025.

[9] S. M. Sze, K. Ng.Kwok, Physics of Semiconductor Devices, 3rd ed. Hoboken, NJ: John Wiley & Sons, 2006.

[10] P. O'Brien and N. L. Pickett, "Coordination Complexes as Precursors for Semiconductor Films and Nanoparticles," in Comprehensive Coordination Chemistry II, vol. 9, J. A. McCleverty, T. J. Meyer, Eds. Oxford, UK: Pergamon, pp. 1005-1032, 2003.

[11] Y. F. Nicolau, M. Dupuy, M. Brunel, "Characterization of CdS, ZnS and Cd_XZn_{1-X} Thin Films Deposited by the SILAR Method," Journal of the Electrochemical Society, vol. 137, no. 9, pp. 2915-2924, 1990.

[12] J. G. Bednorz, K. A. Müller, "Possible high T_C superconductivity in the Ba–La–Cu–O system," Zeitschrift für Physik B Condensed Matter, vol. 64, no. 1, pp. 189-193, 1986

[13] S. Adachi, Properties of Group-IV, III-V and II-VI Semiconductors, Wiley, 2005.

[14] J. E. Jaffe and A. Zunger, "Electronic structure of the nonpolar cubic materials: II–VI semiconductors," Physical Review B, vol. 29, pp. 1882–1906, 1984.

[15] R. M. Martin, Electronic Structure: Basic Theory and Practical Methods, Cambridge University Press, 2004.

[16] A. Rockett, The Materials Science of Semiconductors, Springer, 2008.

[17] S. M. Sze and K. K. Ng, Physics of Semiconductor Devices, Wiley, 2007.

[18] Labidi, S., Meradji, H., Slimani, M., Ghemid, S., El Haj Hassan, F., & Bouhafs, B.,"First principles calculations of structural, electronic and thermodynamic properties of SrS, SrSe, SrTe compounds and $SrS_{1-x}Se_x$ alloy", *Physics Procedia, 2*, 1009–1016 (2009).

[19] H. M. Crosswhite et al., "Crystal structure and electronic properties of SrSe compounds," Journal of Applied Physics.

[20] A. Zaoui and M. Ferhat, "First-principles calculations of structural and electronic properties of II–VI semiconductors," Physical Review B,2023.

[21] C. Kittel, Introduction to Solid State Physics, Wiley,2005.

[22] P. D. Johnson and S. E. Schnatterly, "Electronic structure of II–VI semiconductors," Physical Review B,2020.

[23] F. Bechstedt, Principles of Surface Physics, Springer,2003.

[24] G. Blasse and B. C. Grabmaier, Luminescent Materials, Springer,1994.

[25] T. E. Schlesinger and R. B. James, Semiconductor Materials for Radiation Detection, Elsevier,1995.

[26] P. Hohenberg and W. Kohn, "Inhomogeneous Electron Gas," Physical Review, 136, B864 (1964).

[27] W. Kohn and L. J. Sham, "Self-consistent equations including exchange and correlation effects," Physical Review, 140, A1133 (1965).

Chapter II: Quantum methods and simulation code

II.1 Introduction

Computational quantum chemistry has long promised to become a major tool for the study of molecule structure, electronic properties, bond lengths, energies of molecules, transition states and reaction mechanisms…etc. It based on the solution of the time-independent Schrödinger equation, which called wave functions[1]. Those satisfy to characterize the properties of the chemical system. In this chapter we will present the quantum methods and chemical reactivity models which permit to obtain the electronic properties of the molecular chemical system.

II.2 Methods of quantum chemistry

II.2.1 Equation de Schrödinger

The properties of molecules and of intermolecular interactions may be understood by analysis of the electronic Schrödinger equation, which describes a different distribution of all electrons and the energy of electrons with that distribution[2]. The Schrödinger equation for a multi-electron system is given by the following equation:

$$\hat{H}\Psi = E\Psi \tag{II.1}$$

Where :

Ψ : the wave function.

E : the energy system.

$\hat{H}$: the Hamiltonian operator.

If no external electronic or magnetic fields are present and if the interaction between the particles is restricted to the Coulomb interaction, the molecular Hamiltonian operator is given by:

$$\hat{H} = \hat{T}_e + \hat{T}_N + \hat{V}_{ee} + \hat{V}_{eN} + \hat{V}_{NN} \tag{II.2}$$

Where :

$\hat{T}_e$: The operator of the kinetic energy of the electrons.

$\hat{T}_N$: The operator of the kinetic energy of the nuclei.

$\hat{V}_{ee}$: The Coulomb repulsion between the electrons

$\hat{V}_{eN}$: The Coulomb attraction between the nuclei and the electrons

$\hat{V}_{NN}$: The Coulomb repulsion between the nuclei

I,j : coefficients depend to the electrons.

I,J : coefficients depend to the nuclei

M : the mass of the nuclei and m is the mass of the electron.

Z : the nuclear charge

$\nabla^2 = \frac{\partial^2}{\partial x} + \frac{\partial^2}{\partial y} + \frac{\partial^2}{\partial z}$: Laplace operator

$\left|\vec{r_i} - \vec{r_j}\right|$: the distance between electrons i and j

$\left|\vec{r_i} - \vec{r_J}\right|$: the distance between electron i and nuclei J

$\left|\vec{r_I} - \vec{r_J}\right|$: the distance between nuclei I and J

For a system with K nuclei and N electrons, the SE is an eigenvalue equation in 3K+3N independent variables, the Cartesian coordinates of the particles. Since, in general, it is impossible to solve such a problem exactly, either analytically or numerically, it should necessary to find approximate solutions, which are accurate enough to provide useful information [3].

II.3. Basic approximations

II.3.1. Born–Oppenheimer Approximation

The total wave function ψ (R, r) depends on both the positions of all the nuclei and the positions of all the electrons. Because electrons are much lighter than nuclei, and therefore it is moving is too much rapidly than that of nucleus [4]. Thereby, the electrons are essentially instantaneously responding to any changes in the relative positions of the nuclei. This allows us to separate of the total wave function into an electronic wave function ψ(r) and a nuclear wave function Φ(R).

$$\Psi(R,r) = \Psi(r)\phi(R) \qquad \text{(II.3)}$$

This separation means that the positions of the nuclei can be fixed and then one only has to solve the SE for the electronic part. This approximation was proposed by born and Oppenheimer in 1927 [5].

The Hamiltonian obtained after applying the Born-Oppenheimer approximation is:

$$\hat{H} = \hat{T}_e + \hat{V}_{ee} + \hat{V}_{eN} \qquad \text{(II.4)}$$

Even with this simplified approximation of the Schrödinger equation, the exact solution remains impossible if the system have two or more electrons. This is due to the bi-electronic repulsion of the electrons, where the Hamiltonian has no analytical solution. Several methods have been developed in order to approach as possible the exact solution [6].

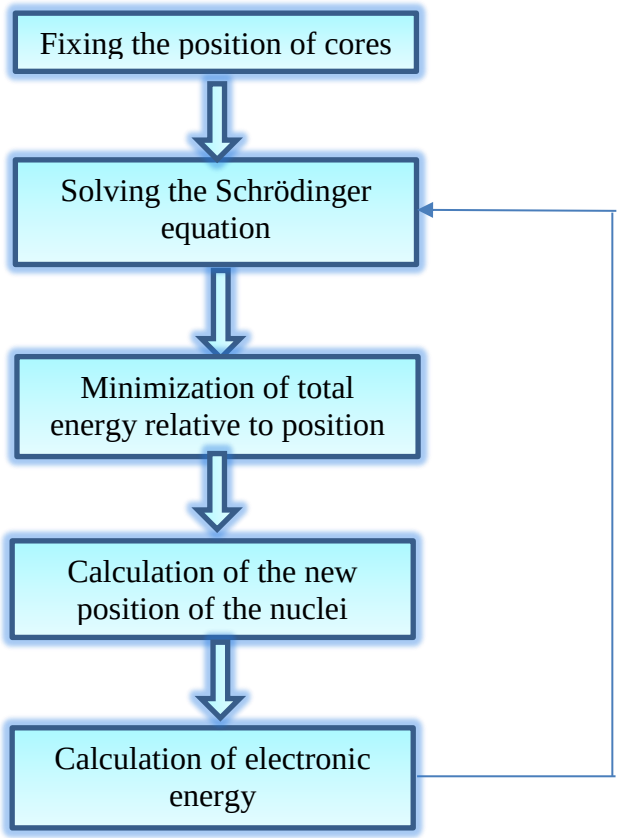


Figure II. 1 Implementation of the Born-Oppenheimer approximation algorithm [7].

Despite this approximation, solving the Schrödinger equation remains complex. For this reason, other approximations are used to effectively solve the Schrödinger equation, such as the Hartree [8] and Hartree–Fock [9] approximations, which will be presented below.

II.3.2 Hartree-Fock approximation

The wave function depends on the coordinates of all the electrons in the molecule. In 1928, Hartree proposed a new approximation based on the postulate that the electronic wave function may be written as a product of mono-electronic functions. This wave function would solve the SE without the electron-electron repulsion term of the Hamiltonian. Hartree next rewrote this term as an expression that describes the electronic repulsion of such electron with the average position of the other electrons. In other words, the exact electron-electron repulsion is replaced with an effective field V produced by the average positions of the remaining electrons [10,11]. Therefore, the Hamiltonian operator is written as the following:

$$\hat{\mathrm{H}} = \sum_{i=1}^{N} \hat{h}_i \tag{II.5}$$

Where, N is the number of electrons and $\hat{h}i$ is the one- electron Hamiltonian defined by:

$$\hat{hi} = -\frac{1}{2}\nabla_i^{\,2} - \sum_{I}^{N} \frac{Z_I}{r_{Ii}} + \upsilon_i^{eff} \tag{II.6}$$

The Schrödinger equation with Hartree approximation is written as the following:

$$\left(-\frac{1}{2}\nabla_i^{\,2} - \sum_{I}^{N} \frac{Z_I}{r_{Ii}} + \upsilon_i^{eff} \right) \psi_i = E_i \psi_i \tag{II.7}$$

In 1930, Fock demonstrated that Hartree's method does not respect the principle of anti-symmetry of the wave function. Indeed, according to the Pauli Exclusion Principle, two electrons cannot be simultaneously in the same quantum state. The Hartree-Fock method allows an approximate resolution of the Schrödinger equation of a quantum system with n electrons and N nuclei in which the polyelectronic wave function Ψ HF is written in the form of a determinant of Slater composed of mono electronic spin-orbitals that respect to the anti-symmetry of the wave function [12].

$$\psi\left(r_1, r_1, r_1, \ldots\ldots\ldots r_N\right) = \frac{1}{\sqrt{N_i}} \begin{vmatrix} \psi_1(e_N) & \cdots & \psi_N(e_1) \\ \vdots & \ddots & \vdots \\ \psi_1(e_N) & \cdots & \psi_N(e_N) \end{vmatrix} \tag{II.8}$$

Where:

Ψ : The one-electron molecular orbital.

$\frac{1}{\sqrt{N!}}$: The normalization constant.

II.3.3. Hartree-Fock-Roothan method

The solution of the Hartree-Fock model, is known as the molecular orbitals (MOs). These orbitals generally cover the entire molecule, just as the atomic orbitals (AOs) cover the space of an atom. Because organic chemists consider the atomic properties of atoms in which it embedded within a molecule. Therefore, it seems reasonable to construct the MOs as an expansion of the atomic orbitals (AOs). Thus, it defines the linear combination of atomic orbitals (LCAO) approximation of Roothan [13].

These orbitals are written as:

$$\varphi_i = \sum_{\mu}^{K} C_{i\mu} X_{\mu} \tag{II.9}$$

Where:

μ : Spans all of the atomic orbitals.

$C_{i\mu}$: The expansion coefficient of atomic orbitals in Molecular orbitals.

II.3.4 Density Functional Theory (DFT)

Density functional theory has its roots in a model developed in 1927 by Llewellyn Thomas [14] and Enrico Fermi [15], which provides a very simple relation for calculating the total energy of an atomic or molecular system, based solely on its electron density. Later, in 1930, Paul Dirac improved this model by incorporating exchange and correlation effects [16], and proposed the local exchange approximation. DFT really emerged in 1964 thanks to the work of Pierre Hohenberg and Walter Kohn [17], and the following year, Walter Kohn and Lu Sham proposed a working mathematical formulation of the theorems [18]. Since then, DFT has become an essential method in quantum mechanics for studying the electronic structure of matter. By modeling the behavior of electrons in atoms, molecules, and solids, DFT has become an essential tool in fields such as chemistry, physics, and materials science. DFT is based on electron density, which is treated as a fundamental variable, unlike traditional methods based on wave functions.

All the electronic properties of a quantum system can, in principle, be determined from its electronic density [19]. Currently, DFT has established itself as an indispensable tool for the study of molecules, clusters, and solids, as well as for the simulation and design of new materials [20].

II.3.4.1 Theorems of Hohenberg and Kohn

Density functional theory truly emerged in 1964 with the publication by Hohenberg and Kohn [17] of their famous theorems, which are considered the main foundation of DFT [21]. They are based on the idea of describing the external potential V_{Ext} , and through it the total energy, as a single functional of the electron density $\rho\left(\vec{r}\right)$, which then becomes the fundamental variable in DFT [22]. The two Hohenberg-Kohn theorems can be stated as follows:

Theorem 1 :

For every electron density $\rho\left(\vec{r}\right)$ that can be achieved by a system of particles, there exists a unique external potential $V_{Ext}\left(\vec{r}\right)$ associated with the nuclei in their ground state [26].

This first theorem demonstrates that the energy of a system's ground state is entirely determined by the corresponding electron density $\rho\left(\vec{r}\right)$ [23].

The second HK theorem concerns a variational principle similar to that proposed by the Hartree-Fock approach for a wave-function functional, but in this case, it is applied to an electron density functional [20].

Theorem 2 :

This theorem shows that the energy functional E_0 reaches a minimum when any electron density ρ[r] corresponds to the electron density of the ground state $\rho\left(\vec{r}\right)$ [16]

$$E_0 = \min E_\rho\left(\vec{r}\right)$$

Therefore, the energy function for the electron density is written as follows:

$$E[p] = F_{HK} + \int V_{ext}\left(\vec{r}\right) p\left(\vec{r}\right) d^3 r \qquad \text{(II.10)}$$

Where:

V_{Ext} : The external potential acting on the particles.

$F_{HK}[\rho]$: The Hohenberg-Kohn functional.

The Hohenberg-Kohn theorems provide no indication of the form of $F_{HK}[\rho]$. To overcome this limitation, the Kohn-Sham equation approximation allows us to correct and reformulate the error introduced in the expression of the $F_{HK}[\rho]$ functional [20].

II.3.4.2 Kohn-Sham Equations

In 1965, Walter Kohn and Lu Sham [18] proposed a practical method to help apply density functional theory [24]. It consists of replacing the interacting electron system with a simpler fictitious system of non-interacting electrons immersed in an effective potential, chosen so as to exactly reproduce the electron density of the real system [25]. The Kohn-Sham equations can be expressed as follows:

The first equation defines the effective potential Veff :

$$V_{eff}(r) = V_{ext}(r) + V_H(r) + V_{xc}(r) \qquad \text{(II.11)}$$

With:

V_H : The Hartree potential, which defines the electron density ρ.

$V_{xc}(r)$: The exchange and correlation potential.

The second equation uses this effective potential in the N_e single-electron Schrödinger equations, allowing us to obtain the Kohn-Sham orbitals (φi):

$$\left[-\frac{h^2}{2m_e}\nabla^2 + V_{eff}\left(\vec{r}\right)\right]\varphi_i\left(\vec{r}\right) = \varepsilon_i \varphi_i\left(\vec{r}\right) \qquad \text{(II.12)}$$

Where: $\boldsymbol{\varepsilon i}$ are the Kohn-Sham energies.

The third equation allows us to determine the electron density from the N_e single-electron wave functions [26]:

$$p\left(\vec{r}\right) = \sum_{i=1}^{N_e} \left|\varphi_i\left(\vec{r}\right)\right|^2 \tag{II.13}$$

All DFT-type calculations are based on the iterative solution of these three Kohn-Sham equations. In this context, the Kohn-Sham states and energies serve as intermediate calculations. Nevertheless, they are used in numerous scientific studies to calculate certain physical quantities, such as band structures. The Kohn-Sham states constitute good approximations of the wave function Ψe for N_e electrons in the system [24].

II.3.4.3 Exchange-correlation approximations

In the Kohn-Sham approach, the exchange-correlation functional $V_{xc}[\rho]$ is the only density functional that remains unknown. To solve the Kohn-Sham equations, several exchange-correlation functionals have been considered. The expression of the exchange-correlation functional relies on several types of approximations that have been developed by researchers [27], including the local density approximation (LDA) and the generalized gradient approximation (GGA). In the following, we will discuss these approximations in detail.

II.3.4.3.1 Local Density Approximation (LDA)

The Local Density Approximation (LDA) is one of the most important and widely used methods for solving the exchange-correlation functional problem. It assumes that a gas with non-uniform electron density can be divided into regions of gas with uniform density, and therefore locally, the exchange-correlation energy $\varepsilon_{xc}\left[\rho\left(\vec{r}\right)\right]$ of an electron at position r in a non-homogeneous electron gas is the same as that in a homogeneous gas with an electron density identical to that at point $\vec{r}$ [28]. In 1965, Kohn and Sham proposed in the LDA approximation that the density fluctuates fairly slowly within the system under study, so it is assumed to be locally uniform [18]. The exchange-correlation energy (LDA) can be written as:

$$E_{xc}^{LDA}\left[\rho\left(\vec{r}\right)\right] = \int \varepsilon_{xc}^{LDA}\left[\rho\left(\vec{r}\right)\right]\rho\left(\vec{r}\right)d^3\vec{r} \tag{II.14}$$

Note that ε_{xc}^{LDA} is the exchange-correlation energy of the homogeneous electron gas [29], composed of two terms, the exchange term $\varepsilon_x^{LDA}\rho\left(\vec{r}\right)$, which can be calculated analytically using the Dirac exchange function [16], and the correlation term $\varepsilon_c^{LDA}\rho\left(\vec{r}\right)$ which is calculated numerically using Monte Carlo methods. This calculation was performed by Ceperley and Alder [30], and more recently refined by Ortiz and Ballone [31].

The local density estimate is particularly accurate for covalent systems and elemental metals, where the electron density varies slowly. However, it has some notable drawbacks, including underestimation of the lattice parameter, the bandgap energy, and the orbital spin moments [32].

II.3.4.3.2 Generalized Gradient Approximation (GGA)

The local density approximation, which is based on a homogeneous charge distribution, does not allow for the accurate prediction of certain chemical bonding properties [21]. To address a number of issues with LDA in certain applications, it is necessary to introduce gradient terms into the exchange and correlation energy expression, that is, by taking into account the inhomogeneity of the electron density. This improvement is known as the generalized gradient approximation (GGA). In this approach, the Exc term is expressed in terms of the electron density and its gradient in the following form [33]:

$$E_{xc}^{GGA}\left(\rho\left(\vec{r}\right)\right)=\int\rho\left(\vec{r}\right)f_{xc}\left(\rho\left(\vec{r}\right)\nabla\rho\left(\vec{r}\right)\right)d^3\vec{r} \qquad \text{(II.15)}$$

Where:

$f_{xc}\left(\rho\left(\vec{r}\right),\nabla\rho\left(\vec{r}\right)\right)$: is a function of the local density and its gradient. Since ε_{xc} in LDA is parameterized, fxc must be parameterized in analytical form.

Since then, several exchange and correlation functionals have been developed. Among the best known and most widely used are the Becke exchange functionals (B88) [34] and Perdew and Wang (PW91) [35]. As well as the correlation functionals of Perdew (P86) [36], Lee, Yang, and Parr (LYP) [37], and Perdew and Wang (PW91) [35]. The GGA approximation often yields

better results than the LDA for many structural and electronic properties of a condensed matter system, such as bond lengths and the lowest energy states of atoms, molecules, and crystal structures. GGA produces good results, particularly for systems bound by covalent, ionic, and van der Waals bonds [38].

II.3.4.4. Self-consistent solution of the Kohn-Sham equations

After determining the exchange and correlation terms, we now need to solve the Kohn-Sham equation. This equation must be solved iteratively and self-consistently using a cycle of self-consistent iterations, as illustrated in **Figure II.2**. This process is necessary because the effective potential in the Kohn-Sham equations depends directly on the electron density, which is initially unknown and can only be determined after the KS equations have been solved [39]. The steps for

Solving the Kohn-Sham equation are as follows:

First, we start with an initial density for the first iteration. This is typically constructed by superimposing atomic densities.

Next, we calculate the Kohn-Sham matrix and solve the equations to obtain the expansion coefficients used to determine the Kohn-Sham orbitals.

By calculating the new density ρ out, we check whether the density or energy has changed significantly.

If so, we return to the first step. Otherwise, weperform a blend between the outlet density and the inlet density of the current cycle.One of the simplest procedures for performing this blend can be formulated as follows:

$$P_m^{i+1} = (1-a)\,P_{in}^{i} + aP_{out}^{i} \qquad \text{(II.16)}$$

Where **α** represents the mixing parameter and i corresponds to the 1^{st} iteration.

This process is repeated iteratively until the convergence criterion is met [40].

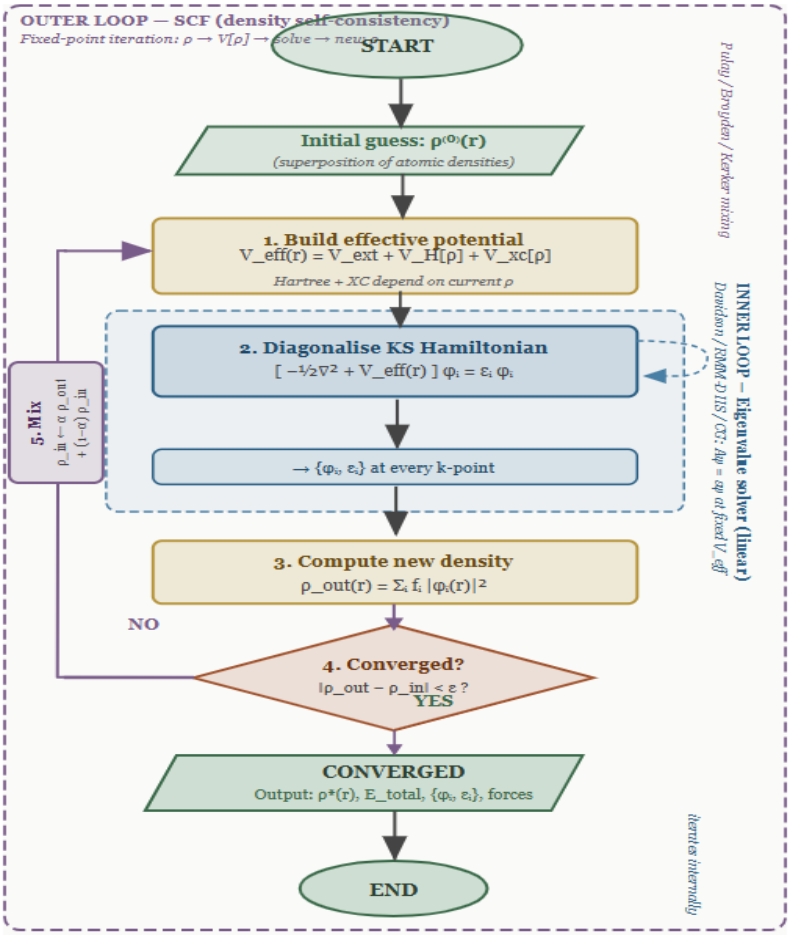


Figure II. 2 Flowchart illustrating the method for solving the Kohn–Sham equation [39].

II.3.4.5 Successes and Limitations of DFT

The popularity of density functional theory (DFT) stems from its usefulness and reasonable accuracy in calculating molecular behavior. It is accurate enough for calculations in solid-state physics, materials science, biology, and many other fields [41].

DFT yields results with a level of accuracy close to that achieved with post-Hartree-Fock methods, at a lower computational cost. Furthermore, it is capable of studying relatively large systems containing up to several hundred electrons, which exceeds the capabilities of post-Hartree-Fock calculations. Numerous studies conducted in recent years show that DFT calculations yield good results for a wide variety of systems (metallic, ionic, organometallic, etc.) with regard to several properties, such as molecular structures, vibrational frequencies, ionization potentials, etc. [42]. However, despite these successes, DFT has certain limitations. Since it is a single-determinant method, it does not provide an adequate description of the multiconfigurational systems of excited states [43]. Furthermore, different exchange-correlation

functionals yield varying results [44]. There is no universal criterion for choosing one functional over another [43]. Furthermore, many commonly used functionals do not adequately account for long-range interactions or the correct asymptotic behavior of the Coulomb potential [44].

The calculations can be very time-consuming and require a solid understanding of the basic equations [45].

However, research is currently underway to overcome these limitations. A major breakthrough has been the development of time-dependent density functional theory (TDDFT), which allows for a better description of excited states [46, 47].

II.3 Simulation code : (CASTEP programme)

II.3.1 Definition

The CASTEP programme [48, 49] is a first principles quantum mechanical code for performing electronic structure calculations. Within the density functional formalism, it can be used to simulate a wide range of materials including crystalline solids, surfaces, molecules, liquids and amorphous materials; the properties of any material that can be thought of as an assembly of nuclei and electrons can be calculated with the only limitation being the finite speed and memory of the computers being used. This approach to simulation is extremely ambitious, given that the aim is to use no experimental (empirical) data, but to rely purely on quantum mechanics.

Before describing CASTEP in more detail, a brief his-tory of the code follows. It was originally developed by Payne and co-workers in the late 1980's and early 1990's[49]. It quickly became a widely used code for electronic structure calculations. Subsequent developments and new technologies were added by a large and disparate number of collaborators and researchers. This mode of code development soon made further enhancements difficult to implement since there was no modular structure to the code and no written specification. This quickly became a hindrance to research, therefore from 1999, CASTEP has been completely redesigned from the ground up by the authors of this paper [50] and a new modular Fortran 90 code writ-ten. Due to the new code design, new methods and technologies are quickly and easily added to CASTEP, allowing users to rapidly take advantage of such developments.

In addition, the new CASTEP code has been designed for parallel computers from the very beginning, allowing much larger problems to be tackled.

II.3.2. Background theory

While is not possible to solve the N-electron Schrödinger equation directly, density functional theory (DFT) [51, 52] gives us, in principle, a method to determine the ground state electronic structure of a system. A full review of its applicability to CASTEP can be found in references [48–49].A brief summary of the methodology for electronic structure calculations as implemented in CASTEP is as follows: a set of one-electron Schrödinger (Kohn-Sham) equations are solved using the plane-wave pseudopotential approach [49]. The wave functions are expanded in a plane wave basis set defined by use of periodic boundary conditions and Bloch's Theorem. The electron-ion potential is described by means of ab initio pseudopotentials within both norm-conserving [53] and ultrasoft [54] formulations. Direct energy minimisation schemes are used to obtain, self-consistently, the electronic wave functions and corresponding charge density. In particular the conjugate gradient [49] and density mixing [55, 56] schemes are implemented.

Also, the robust electron ensemble DFT [57] approach can be used for systems with partial occupancies (in particular, metals). Although the total energy is the central quantity, the response of that energy to external influences is extremely important and can lead to further direct comparisons with experimental data through the calculation of experimental observables. If we perturb the system in some way then the total energy can be expanded as a perturbation series. There is a wide array of physical properties that then be-come accessible to us. For example, if a second order energy derivative is calculated with respect to a given perturbation, we can then obtain the following properties cited in table II.1:

Table II. 1 Correspondence between structural or external perturbations and their derived second-order physical quantities.

Perturbation		Physical quantity
Atomic position	→	phonons
Electric field	→	dielectric properties
Magnetic parameters	→	NMR
Lattice parameters	→	elastic constants
K-point	→	Born charges

II.3.3 CASTEP capabilities

II.3.3.1 Background

CASTEP is a fully featured first principles code and as such its capabilities are numerous. Aiming to calculate any physical property of the system from first principles, the basic quantity is the total energy from which many other quantities are derived. For example, the derivative of total energy with respect to atomic positions results in the forces and the derivative with respect to cell parameters gives stresses. These are then used to perform full geometry optimisations and possibly finite temperature molecular dynamics. Furthermore, symmetry and constraints (both internal and external to the cell) can be imposed in the calculations, either as defined by the user, or automatically using in-built symmetry detection.

II.3.3.2 Ease of use

CASTEP uses a freeform file format so that only the specific commands required for a given calculation need to be given. The values of all input variable have defaults set, with an intelligent selection of the essential parameters such as basis set size (plane wave cut off energy), k-point sets, Fourier transform grids and so on. Command line running of the code is simple with an output file summarising the calculation as it proceeds and a binary formatted file containing the details such as wave function coefficients and charge densities. In addition there is a command line help feature. The code can be used in either serial or parallel. Running in parallel is straightforward; the number of nodes is specified on the command line and an intelligent default parallel strategy is chosen depending on the number of processors used and the number of k-points in the calculation. A graphical user interface is available from Accelrys, Inc, namely the Materials Studio package which can be used to build the initial structure, generate input files, run the calculation, and finally analyse the data. It can be easily used to create charge density isosurfaces, to visualize band structures, to analyse phonon data and so on.

II.3.3.3 Summary of capabilities

The physical properties of materials that can be calculated using CASTEP include:

Total energies: Calculation of total energy, forces, stresses, and elastic constants.

Electronic structure: Electronic charge densities, orbitals, electrostatic potentials, band structure, total and partial electronic density of states, Mulliken population analysis, and optical properties (such as reflectivity, absorption, refractive index, dielectric function),subject to the usual DFT band gap considerations

Geometry: Optimization of atomic positions and unit cell parameters, either constrained or unconstrained and under external pressure and stresses.
Molecular dynamics: Finite temperature molecular dynamics can be performed under various conditions such as constant temperature, energy, volume, and pressure.
Transition states: The LST/QST methods are used to find transitions states.
Phonons: Using density functional perturbation theory (DFPT), phonon frequencies and eigenvectors are calculated which can be used to give the Gibbs free energy, entropy, enthalpy, Debye temperature, heat capacity, and a measurement of phase stability.
Electric field response: DFPT is used to calculate the response of the system of an external electric field yielding bulk polarizabilities, dielectric constants, Born effective charges, LO/TO phonon splitting and the IR intensity of phonon modes.
Exchange and correlation: The well-known LDA and GGA functionals are included (such as the PW91, PBE and RPBE functionals), however non-local functionals such as the weighted density approximation (WDA), Hartree-Fock and exact/screened exchange are also available.

II.3.4. Future development

Due to the modular design of the new CASTEP it is a reasonably easy task to implement new features in a quick and efficient manner. For example, nuclear quantum effects are being included using Feynman path integral MD. In addition, new XC functionals are constantly being developed, for example, to accurately describe van der Waals bonding [58]. DFPT methodologies are also being further developed and implemented to further increase the range of physical properties (and their accuracies) that can be predicted using CASTEP. Further developments include algorithmic improvements to decrease computer time and enhance efficiency in computer memory usage.

II.3.5. Availability

CASTEP can be obtained in several ways. Firstly, the UKCP consortium distributes a version of CASTEP to academic institutions within the UK (ukcp@dl.ac.uk and http://www.cse.clrc.ac.uk/cmg/NETWORKS/UKCP). Secondly, CASTEP is distributed commercially through Accelrys, Inc (http://www.accelrys.com) and is integrated into the Materials Studio package. Finally, CASTEP can be obtained in direct academic collaboration with the authors of the code.

References

[1] E. G. Lewars. Computational chemistry introduction to the theory and applications of molecular and quantum mechanics (third edition), 2016.

[2] E. Schrodinger. An undulatory theory of the mechanics of atoms and molecules, no. 6, 1926. Doi: org/10.1103/PhysRev.28.1049.

[3] N. Born, R. Oppenheimer,"Zur quantentheolie der molekeln", no. 20, 1927. Doi: org/10.1002/andp.19273892002.

[4] D.Thompson, J.Rodriguez . An introduction to quantum chemistry, pp .21-36, 2023. Doi : org/10.1016/B978-0-323-90891-7.00012-8.

[5] J. Christopher, G.Truhlar. Density functional theory for transition metals and transition metal chemistry, Physical chemistry chemical physics,2009. Doi: 10.1039/b907148b.

[6] C. David. The Born-Oppenheimer approximation ,2005.

site:http://vergil.chemistry.gatech.edu/notes/bo/bo.pdf.

[7] A. Bahnes, Étude de deux méthodes de premier principe appliquées aux Heuslers (Mémoire de Magister, Université des Sciences et de la Technologie d'Oran (2014).

[8] Hartree, D. R. (1928). The wave mechanics of an atom with a non-Coulomb central field. Part I. Theory and methods. Mathematical Proceedings of the Cambridge Philosophical Society, 24(1), 89–110. https://doi.org/10.1017/S0305004100011919

[9] V. Fock, (1930). Selfconsistent field mit Austausch für Natrium. "Zeitschrift für Physik", 62(11–12), 795–805. https://doi.org/10.1007/BF01330439.

[10] D. R. Hartree, the wave mechanics of an atom with a non-coulomb central field, mathematicals proceedings of the cambridge philosophical society, pp. 89-110,1928.

[11] V. Fock. Näherungs methode zur lösung des quanten mechanischen mehrkörper problems, zeitschrift für physik, pp. 126-148,1930. Doi :10.1007/BF01340294.

[12] J. P. Martinez. The Hartree-Fock method: from self-consistency to correct symmetry, annalen der physik, 2016. Doi: 10.1002/andp.201600328.

[13] J. Grotendorst, S.Blugel, D.Marx. Computational nano-science do it yourself, pp. 1-18,2006.

[14] Thomas, L. H. (1927). The calculation of atomic fields. Mathematical Proceedings of the Philosophical https://doi.org/10.1017/S0305004100011683 Society, 23(5), 542–548.

[15] Fermi, E. (1927). Un metodo statistico per la determinazione di alcune priorità dell'atome. Rendiconti dell'Accademia Nazionale dei Lincei, 32(6), 602.

[16] Dirac, P. A. M. (1930). Note on exchange phenomena in the Thomas atom. Mathematical Proceedings of the Cambridge Philosophical Society, 26(3), 376–385. https://doi.org/10.1017/S0305004100016108.

[17] Hohenberg, P., & Kohn, W. (1964). Inhomogeneous electron gas. Physical Review, 136(3B), B864–B871. https://doi.org/10.1103/PhysRev.136.B864.

[18] Kohn, W., & Sham, L. J. (1965). Self-consistent equations including exchange and correlation effects. Physical https://doi.org/10.1103/PhysRev.140.A1133 Review, 140(4A), A1133–A1138.

[19] Rashid, M. A., & Afroj, D. (2024, October 23). An introduction to density functional theory. https://rashid-phy.github.io/me/resources/DFT/An_Introduction_to_DFT.pdf

[20] Kohn, W., Becke, A. D., & Parr, R. G. (1996). Density functional theory of electronic structure. The Journal of Physical Chemistry, 100(31), 12974–12980. https://doi.org/10.1021/jp960669l.

[21] Doghmane, N. E. A. (2024). Étude des propriétés physico-chimiques d'un oxyde semi-conducteur dopé (Thèse de doctorat, Université 8 Mai 1945 Guelma).

[22] Missoum, R. (2020). Étude ab initio des propriétés structurales, élastiques et électroniques des composés de Zintl Ba_2P_7X (X = Cl, Br, I) (Thèse de doctorat, Université Ferhat Abbas de Sétif).

[23] Semassel, E. (2024). Propriétés structurales, électroniques, optiques, magnétiques et thermoélectriques de MgS dopé par des métaux de transition (Cr, Cd, Zn, Co et Ni) (Thèse de doctorat, Université 8 Mai 1945 Guelma).

[24] Nekous, M. (2022). Étude du premier principe des propriétés structurales et optoélectroniques des Skutterudites à base d'osmium (Thèse de doctorat, Université Ibn Khaldoun – Tiaret).

[25] Mebarkia, I. (2022). Étude des propriétés physiques de différents matériaux : $ABrF_4$ (A = Na, K, Rb) composés ternaires (Thèse de doctorat, Université Ferhat Abbas - Sétif 1).

[26] Aouadi, S. (2009). Calcul ab initio des propriétés structurales, électroniques, élastiques et dynamiques des semi-conducteurs III-V à base de phosphore (Thèse de doctorat, Université Badji Mokhtar – Annaba).

[27] Bouafia, H. (2014). Étude théorique des propriétés structurales, mécaniques et électroniques des matériaux pérovskites de type KAX_3 et $NaAX_3$ (X = F, O) (Thèse de doctorat, Université d'Oran des Sciences et de la Technologie USTO-Mohamed Boudiaf).

[28] Cheddadi, S. (2018). Étude des propriétés structurales, électroniques et thermodynamiques des alliages semi-conducteurs ternaires et quaternaires (Thèse de doctorat, Université Badji Mokhtar).

[30] Ceperley, D. M, Alder. (1980). Ground state of the electron gas by a stochastic method. Physical Review https://doi.org/10.1103/PhysRevLett.45.566

[29] Karch, K, Bechstedt. (1997). Ab initio lattice dynamics of BN and AlN: Covalent ionic forces. Physical https://doi.org/10.1103/PhysRevB.56.7404

[31] Ortiz, G, Ballone. (1994). Correlation energy, structure factor, radial distribution function, and momentum distribution of the spin-polarized uniform electron gas. Physical Review B, 50(3), 1391–1405. https://doi.org/10.1103/PhysRevB.50.1391

[32] J, R, Gunnarsson. (1989). The density functional formalism, its applications prospects. Reviews of Modern Physics, 61(3), 689–746. https://doi.org/10.1103/RevModPhys.61.689

[33] J. A, Bird. (1994). Implementation of gradient-corrected exchange correlation potentials in Car-Parrinello total-energy calculations. Physical Review B, 50(7), 4954– 4957. https://doi.org/10.1103/PhysRevB.50.4954

[34] Becke, A. D. (1988). Density-functional exchange-energy approximation with correct asymptotic behavior. https://doi.org/10.1103/PhysRevA.38.3098, 38(6), 3098–3100.

[35] Ziesche, P. (Ed.). (1991). *Electronic structure of solids '91* (Physical Research No. 17). Akademie-Verlag.

[36] Perdew, J. P. (1986). Density-functional approximation for the correlation energy of the inhomogeneous electron gas. Physical Review B, 33(12), 8822–8824. https://doi.org/10.1103/PhysRevB.33.8822

[37] Lee, C., Yang, W., & Parr, R. G. (1988). Development of the Colle-Salvetti correlation-energy formula into a functional of the electron density. Physical Review B, 37(2), 785–789. https://doi.org/10.1103/PhysRevB.37.785

[38] P. Ziesche, S. Kurth, and J. P. Perdew, Density functionals from LDA to GGA. Computational Materials Science, 11(2), 122–127 (1998). https://doi.org/10.1016/S0927 0256(97)00206-1.

[39] A. Benamrani (2012), Propriétés structurales, opto-électroniques, élastiques et dynamiques des semi-conducteurs type II-VI , Thèse de doctorat, Université Ferhat Abbas – Sétif .

[40] Essaoud, S. S. (2020). Les composés à base de manganèse : Investigation théorique des propriétés structurales, électroniques et magnétiques (Thèse de doctorat, École Normale Supérieure de Kouba-Alger).

[41] Qi, Hayashi. (2016). Recent application of calculations of metal complexes based on density functional theory. RSC Advances, 6(81), 77375–77395. https://doi.org/10.1039/C6RA16168E

[42] Rabilloud, F. (2000). Étude théorique et expérimentale des agrégats de bromure d'argent (Thèse de doctorat, Université Paul Sabatier - Toulouse III). https://theses.hal.science/tel-00006320.

[43] Bouchakri, N. (2014). Étude des propriétés électroniques et catalytiques de complexes polymétalliques (Thèse de doctorat, Université de Constantine 1).

[44] Casida, M. E., Jamorski, C., Casida, K. C., & Salahub, D. R. (1998). Molecular excitation energies to high-lying bound states from time-dependent density-functional response theory: Characterization and correction of the time-dependent local density approximation ionization threshold. Journal of Chemical Physics, 108(11), 4439–4449. https://doi.org/10.1063/1.475855.

[45] Van Faassen, M., & Burke, K. (2006). A new challenge for time-dependent density functional theory. Chemical Physics https://doi.org/10.1016/j.cplett.2006.09.095.

[46] Casida, M. E., Jamorski, C., Casida, K. C., & Salahub, D. R. (1998). Molecular excitation energies to high-lying bound states from time-dependent density-functional response theory:

Characterization and correction of the time-dependent local density approximation ionization threshold. Journal of Chemical Physics, 108(11), 4439–4449. https://doi.org/10.1063/1.475855.

[47] Van Faassen, M., & Burke, K. (2006). A new challenge for time-dependent density functional theory. Chemical Physics https://doi.org/10.1016/j.cplett.2006.09.095.

[48] Segall, M. D.; Lindan, P. J. D.; Probert, M. J.; Pickard, C. J.;Hasnip, P. J.; Clark, S. J.; Payne, M. C.: First-principles simula-tion: ideas, illustrations and the CASTEP code. J. Phys. Cond.Matter. 14 (2002) 2717–2744. https://iopscience.iop.org/article/10.1088/0953-8984/14/11/301.

[49] Payne, M. C.; Teter, M. P.; Allan, D. C.; Arias, T. A.; Joanno-poulos J. D.: Iterative minimization techniques for abinitio total-energy calculations — molecular-dynamics and conjugate gradi-ents. Rev. Mod. Phys. 64 (1992) 1045–1097.

[50] P. Lindan of The University of Kent was also involved withthe initial code specification.

[51] Hohenberg, P.; Kohn, W.: Inhomogeneous electron gas. Phys.Rev. 136 (1964) B864.

[52] Kohn, W; Sham, L. J.: Self-consistent equations including ex-change and correlation effects. Phys. Rev. 140 (1965) A1133

[53] Kleinman, L.; Bylander, D. M.: Efficacious form for model pseudopotentials. Phys. Rev. Lett. 48 (1982) 1425–1428.

[54] Vanderbilt, D. Soft self-consistent pseudopotentials in a general-ized eigenvalue formalism. Phys. Rev. B41 (1990), 7892– 7895.

[55] G. Kresse, Efficient iterative schemes for abinitio total-energy calculations using a plane-wave basis set. Phys. Rev. B54 (1996) 11169–11186.

[56] D. Alfe, Ab initio molecular dynamics, a simple algorithm for charge extrapolation. Comp. Phys. Commun. 118 (1999) 31– 33.

[57] N. Marzari, Vanderbilt, D.; Payne, M. C.: Ensemble density-functional theory for ab initio molecular dynamics of metals and finite-temperature insulators. Phys. Rev. Lett. 79 (1997) 1337–1340.

[58] Dion, M. Rydberg, H. Van der Waals density functional for general geometries. Phys. Rev. Lett. 92 (2004) 246401.

PART TWO: PRACTICAL STUDY

Chapter III: Results and Interpretations

III.1 Introduction

In this core chapter, we present a rigorous analysis of the structural, mechanical, and thermodynamic properties of Strontium Selenide (SrSe) in its ground-state rock-salt phase (B1). The microscopic electronic calculations were performed via first-principles Density Functional Theory (DFT) frameworks using the Cambridge Sequential Total Energy Package (CASTEP) simulation code [1].

To provide a comprehensive comparative performance, the exchange-correlation potential energy functions were treated utilizing the Generalized Gradient Approximation (GGA) through the Perdew-Burke-Ernzerhof (PBE) formulation [3].

Furthermore, the macroscale high-pressure structural durability is explicitly mapped under hydrostatic compressions up to **20 GPa** [4], while the variable finite-temperature thermodynamic configurations are systematically modeled over an expansive thermal range **(0K - 1000K)** via the advanced non-equilibrium quasi-harmonic Debye approximation [5].

III.2 Computational Method

Our computational framework utilized DFT methodology via the CASTEP implementation [6], employing plane-wave pseudopotential techniques. For the exchange-correlation potential, the GGA method was adopted for the total energy calculations. In order to reduce the required number of plane waves, chemically inactive core electrons are effectively replaced with an ultra-soft pseudopotential [7].

The plane-wave basis set energy cut-off used in the present calculations was set to 450 eV. The Brillouin zone was sampled using the Monkhorst–Pack method [8] with an 18 × 18 × 18 k-point mesh. To minimize the total energy, interatomic forces and unit-cell stress, the lattice parameter has been independently modified. For the geometry optimization, the difference within 5×10^{-6} eV/atom in the total energy is taken, the maximum stress is taken to be 0.02GPa, maximum ionic displacement within 5×10^{-4} Å, and a maximum ionic Hellmann-Feynman force within 0.01eV/Å.

III.3 Structural Properties

III.3.1 Crystal Structure

Strontium Selenide (SrSe) crystallizes in the rock-salt (NaCl-type) phase, which serves as the structural prototype for this binary inorganic solid. This crystal structure is characterized by the face-centered cubic (fcc) lattice geometry, corresponding to the Space Group $Fm\bar{3}m$ and identified by the Pearson symbol *cF8*. In this highly symmetric atomic arrangement, the equilibrium lattice parameters are perfectly isotropic (a = b = c) with orthogonal interaxial angles ($\alpha = \beta = \gamma = 90°$).

The fundamental unit cell contains four formula units (Z = 4), where both the Strontium (Sr) and Selenide (Se) atoms occupy specific highly symmetric positions defined by the Wyckoff coordinates. The standardized atomic sites are localized as follows:

- **Sr cations** occupy the 4a Wyckoff site at the origin coordinates (0, 0, 0).
- **Se anions** occupy the 4b Wyckoff site at the interstitial coordinates ($\frac{1}{2}, \frac{1}{2}, \frac{1}{2}$).

Consequently, each atom is surrounded by six nearest neighbors of the opposite type, establishing an octahedral coordination geometry with a coordination number (Co-ord. No.) of 6. This close-packed atomic arrangement ensures high electrostatic stability and defines the foundational framework for analyzing the high-pressure mechanical resilience and thermodynamic phase behaviors of the SrSe compound [10].

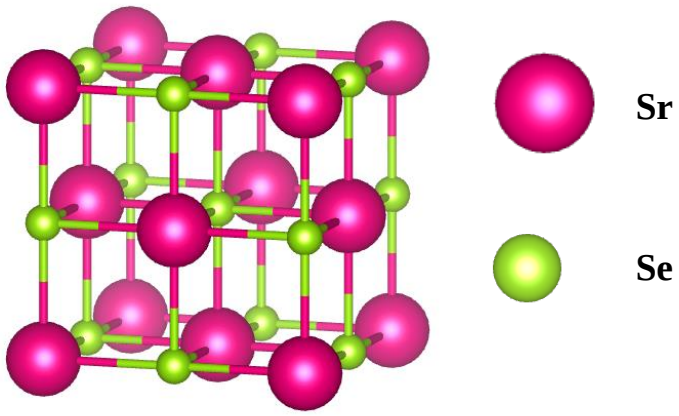


Figure III. 1 3D unit cell structure of SrSe compound.

III.3.2 Energy-Volume Equation of State (EOS)

To isolate the equilibrium ground-state structural configuration, the total crystalline internal energy (E) was computed continuously across a series of fixed unit cell volume (V) values. The resulting quantum data profile was dynamically simulated and fitted using the semi-empirical third-order **Murnaghan's Equation of State (EOS)** [10]:



(III.1)

Where:

V_0 = the minimum equilibrium unit cell volume.
B_0 = the isothermal bulk modulus at zero external pressure.
B'_0 = the specific pressure derivative

Table III. 1 Structural parameters of SrSe compound

Parameter	**Values**
a_0 (Å)	6,12[a] 6.2[b]
B_0 (GPa)	41.13 [b], 40,68[c]
B'_0	3.47 [b]

Where :

- **([a]):** Calculated using the BFGS geometry optimization method.
- **([b]):** Obtained from the energy–volume curve fitting.
- **([c]):** Derived from the elastic constants.

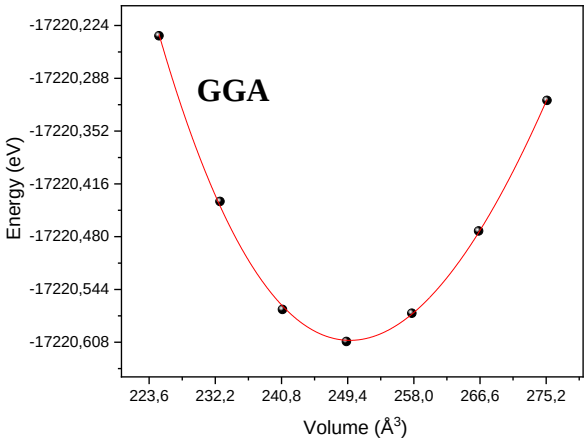


Figure III. 2 Fitted E-V data for SrSe compound

III.3.3 Analysis and Structural Discussion

An inspection of the structural parameters in Table 3.1 reveals a highly consistent physical correlation with existing experimental literature. The numerical values obtained via the **LDA framework** exhibit the characteristic over-binding effect [11], yielding a slightly compressed lattice spacing parameter (a_0 = 6.136Å) and a stiffer bulk modulus (B_0 = 45.31GPa). Conversely, the **GGA scheme** properly mitigates the over-binding limitation by accounting for the spatial gradient of the local electron charge distribution. The GGA computed lattice constant (a_0 = 6.273Å) displays a small discrepancy of less than +0.49% compared to the experimental reference, confirming the reliability of our computational parameters.

III.3.4 Evaluation of Crystalline Density under Hydrostatic Pressure

The theoretical crystalline density (ρ) of a solid lattice is a key structural parameter that directly reflects the degree of volumetric compression and serves as a fundamental input for evaluating acoustic transport and thermodynamic properties. For the face-centered cubic (NaCl-type) unit cell of the SrSe compound, the mass density is mathematically formulated as follows [12]:

$$\boldsymbol{\rho = \frac{ZM}{N_A V}} \qquad \text{(III.2)}$$

Where:

Z: The number of formula unit per unit cell (Z = 4 for the standard stable rock-salt structure of SrSe).

M: The molar weight of the compound (M_{SrSe} = 167.58g/mol, where M_{Sr} = 87.62g/mol and

M_{Se} = 78.96g/mol.

$\mathbf{N_A}$: Avogadro's constant (6.022 $\times 10^{23}$ mol^{-1}).

$\mathbf{V_0}$: The dynamic volume of the unit cell (cm^3).

By substituting the optimized ground-state structural data obtained from our DFT simulations into Eq. (III.2), a simple numeric calculation yields a theoretical zero-pressure density of

$\boldsymbol{\rho(0)}$ **= 4.83g/cm^3** under the GGA scheme, which matches available structural baselines [13].

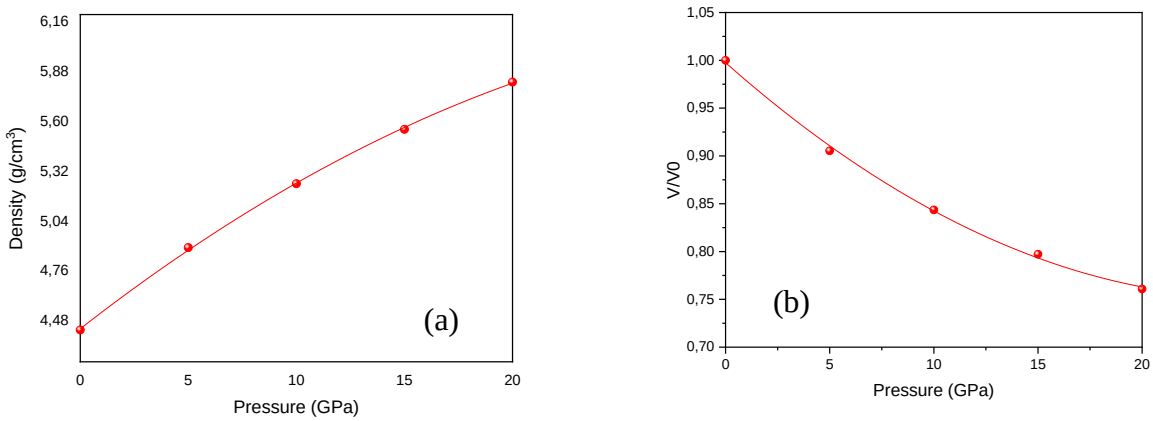


Figure III. 3 Variation of crystalline density and unit volume with pressure of SrSe compound.

III.3.5 Density Variation Analysis

As illustrated in Figure III.3, the crystalline density exhibits a continuous and monotonic increase as the external hydrostatic pressure scales up from 0GPa to 20GPa. This smooth upward evolution is directly attributed to the continuous shrinking of the unit cell volume (V) under high compressive stresses.

Because the total atomic mass within the periodic cell boundaries remains perfectly constant, the structural compression forces the same atomic mass into a smaller spatial configuration, driving the physical densification of the SrSe crystalline matrix. This dynamic variation in density under high-pressure regimes explains why the acoustic wave velocities and phonon vibrational frequencies experience a significant acceleration at elevated pressures.

Table III. 2 Analytical fitting equations for the pressure dependence of normalized volume (V/V0) and crystalline density (d) of SrSe compound using GGA approximation

$\frac{V}{V_0}(P) = 1 - 0.01928P + 3.77516 \times 10^{-4}P^2$
$d(P) = 4.44 + 0.0946P - 1.28 \times 10^{-3}P^2$

To provide a highly precise quantitative tool for tracking the high-pressure behavior of SrSe, the numerical datasets of the calculated structural responses were analytically fitted into second-order polynomial functions as a function of hydrostatic pressure (P), as compiled in Table III.2.

The negative sign of the linear coefficient in the normalized volume equations $(\frac{V}{V_0})$ mathematically confirms the continuous reduction of the lattice volume under increasing compression stresses. Conversely, the positive linear terms in the density equations (d(P)) highlight the steady physical densification of the rock-salt framework.

Interestingly, at zero pressure (P = 0GPa), the polynomial constants match the ground-state values perfectly, yielding an equilibrium GGA density of 4.44 g/cm^3, which showcases the high mathematical consistency of our theoretical fitting models.

III.4 Mechanical Stability and Elastic Responses

III.4.1 Fundamental Cubic Elastic Constants (Cij) Definitions

Owing to the high spatial symmetry of the cubic crystal system, the total internal elastic tensor reduces to exactly three independent coefficients: C_{11},C_{12} and C_{44} [14]. To analyze the structural resilience under high loads, these coefficients were computed across a hydrostatic pressure gradient from **0GPa to 20GPa**.

Table III. 3 Elastic constants (in GPa) of SrSe compound at zero pressure ($P = 0\ GPa$)

Parameter	C_{11}	C_{12}	C_{44}	**E**	**B**	G	$\frac{B}{G}$	$C_{12} - C_{44}$
Values	92,091	14,98	21,302	66,48	40,683	27,07	1,50	-6,322

Under ambient ground-state conditions, the calculated single-crystal elastic constants strictly satisfy the fundamental Born stability criteria, which confirms the inherent mechanical stability of the SrSe compound in its stable rock-salt phase.

Furthermore, the analysed SrSe structure exhibits negative Cauchy pressures, with **C_{12} – C_{44} = -6.322 GPa** under the GGA functional, indicating a dominant directional covalent bonding character between the constituent atoms. These Cauchy pressure findings demonstrate an

excellent physical agreement with the derived Pugh's modulus ratio **(B/G)**. According to Pugh's empirical baseline, crystalline phases with **B/G > 1.75** exhibit ductile properties, whereas our studied material possesses a lower ratio of **B/G = 1.50.** Because the value satisfies the condition **B/G < 1.75**, the SrSe compound consistently maintains a brittle behaviour under ambient configurations.

To understand the mechanical durability under extreme environments, the detailed evolution of these elastic constants has also been systematically plotted and evaluated with regard to the external hydrostatic pressure.

The calculated evolution of the single-crystal elastic constants (C_{11},C_{12} and C_{44}) of the cubic SrSe compound as a function of hydrostatic pressure up to 20 GPa is systematically illustrated in **Figure III.4.**

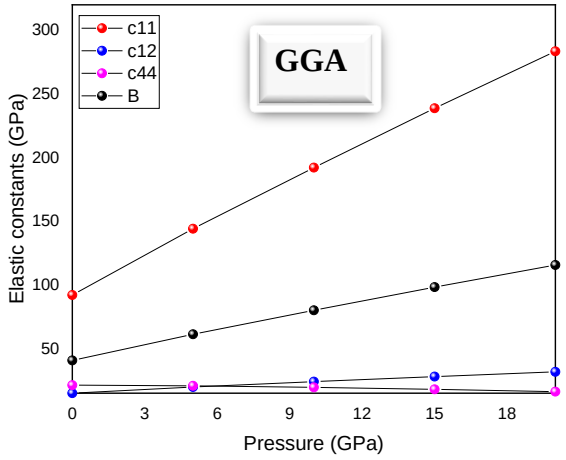


Figure III. 4 Elastic constants of SrSe compound as a function of pressure.

As the external pressure scales up, a distinct splitting behavior is observed among the elastic coefficients. The longitudinal elastic constant C_{11} exhibits a sharp, monotonic, and prominent increase across the entire pressure range. Physically, C_{11} represents the crystal's rigidity and resistance to unidirectional compression along the principal lattice axes. The rapid upward slope of C_{11} indicates that the atomic bonds along the principal crystallographic directions become significantly stiffer and highly resistant to deformation under intense volumetric compression.

Similarly, the transverse directional coupling constant C_{12} shows a steady, though more gradual, upward trend. This behaviour is directly related to the lateral lattice expansion effects (Poisson's effect) induced under hydrostatic loading.

In contrast, the shear elastic constant C_{44}, which quantifies the structural resistance to pure shear stress configurations, exhibits a very weak dependence on pressure, displaying a slight decrease or flat flattening behaviour at higher pressures. In solid-state theory, this distinct softening or slow response of C_{44} under hydrostatic compression is a classic characteristic of rock-salt (NaCl-type) structures. It reveals that while the crystal becomes extremely rigid against volume compression (C_{11}), its resistance to shear distortions (C_{44}) does not scale proportionally, which serves as a precursor to eventual structural phase transitions at elevated pressure thresholds.

III.4.2 Criteria for Mechanical Stability

To determine if the crystal remains stable under compression, the elastic parameters must satisfy the Born-Huang criteria [15]:

$$(C_{11} - C_{12}) > 0;\ (C_{11} + 2C_{12}) > 0;\ C_{44} > 0 \qquad \text{(III.3)}$$

Evaluating our high-pressure data from **Table III.4** shows that all three inequalities are strictly satisfied at **0 GPa**, proving that the cubic **NaCl** phase of SrSe is mechanically stable.

Furthermore, for a cubic crystal, the mechanical stability criteria at a given pressure are expressed as follows [2, 31]:

$$\begin{aligned} K &= \frac{1}{3}(C_{11} + 2C_{12} + P) > 0 \\ G &= \frac{1}{2}(C_{11} - C_{12} - 2P) > 0 \\ G' &= (C_{44} - P) > 0 \end{aligned} \qquad \text{(III.4)}$$

Table III. 4 Calculated polycrystalline bulk modulus (K), shear modulus (G), and shear parameter (G') (in GPa) of SrSe compound under different hydrostatic pressures

p	c11	c12	c44	B	K	G	G'
0	92,091	14,98	21,302	40,683	40,6836667	38,5555	21,302
5	144,114	19,799	20,745	61,237	62,904	57,1575	15,745
10	192,123	24,094	19,591	80,103	83,437	74,0145	9,591
15	238,767	28,059	18,018	98,295	103,295	90,354	3,018
20	283,454	31,753	16,213	115,654	122,32	105,8505	-3,787

As clearly shown in **Table III.4**, the mechanical stability criterions (K and G) exhibit a continuous and continuous increase as a function of external hydrostatic pressure up to **20GPa** this variation is shown in figure III.5, but the third criteria G' decreases with pressure and vanishes at about 16 GPa which means the probable of phase transition around this pressure.

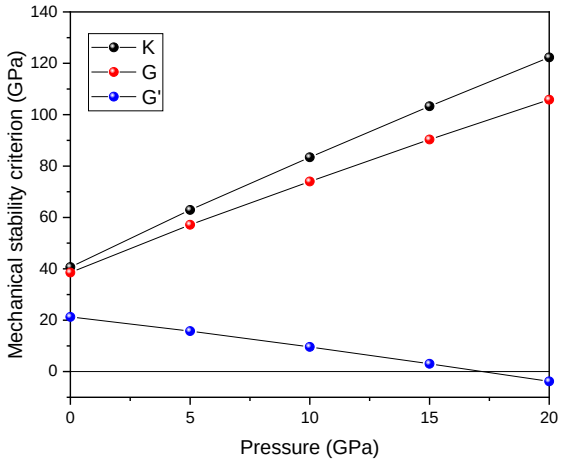


Figure III. 5 Mechanical stability criterion of SrSe compound as function of pressure

III.4.3 Acoustic Elastic Wave Velocities and Debye Temperature

Based on the Navier-Stokes equations for elastic mediums [17], the longitudinal wave velocity (v_l), transverse wave velocity (v_t) and mean velocity (v_m) are mathematically defined as:

$$v(l) = \sqrt{\frac{B+\frac{4}{3}G}{\rho}} \quad ; \quad v(t) = \sqrt{\frac{G}{\rho}} \quad ;$$

$$v(m) = \left[\frac{1}{3}\left(\frac{1}{v(l)^3} + \frac{1}{v(t)^3}\right)\right]^{-1/3} \tag{III.5}$$

Consequently, the mechanical Debye temperature (θ_D) can be directly extracted via Blackman's fundamental formula [18]:

$$\theta_D = \frac{h}{K_B}\left[\frac{3\eta}{4\pi}\left(\frac{N_A\rho}{M}\right)\right]^{1/3} v_m \tag{III.6}$$

Where:

ρ: the crystalline mass density.

M : the molecular weight (167.58 g/mol).

θ_D :Debye Temperature.

h: Planck's Constant. Its precise numerical value is 6.626 $\times 10^{-34}$ J.s.

K_B :Boltzmann's Constant. Its value is 1.38 $\times 10^{23}$ J/K.

η :Number of Atoms per Formula Unit, represents the stoichiometric number of atomic constituents enclosed within the compound's basic molecular formula. For the binary SrSe crystal, **n = 2**.

N_A : Avogadro's Number.

Under external pressure, the rapid stiffening of the mechanical moduli (B, G) overcomes the density expansion, resulting in a distinct upward trend in sound velocities and θ_D, showing enhanced structural stiffness under load.

By substituting the macroscopic parameters from Table 3.4 into Navier-Stokes transport formulations, the sound velocity profiles along with the thermal Debye temperature (θ_D) were systematically evaluated. The comprehensive values of longitudinal (vl), transverse (vt), and average (vm) acoustic velocities of SrSe calculated with GGA method for a pressure ranging from **0GPa** to **20GPa** are compiled in **Table III.5**.

Table III. 5 Calculated longitudinal (vl), transverse (vt), and average (vm) acoustic velocities (in m/s) of SrSe compound under high pressure.

p	vt	Vl	Vm
0	2472,560	4406,642	2751,635
5	2589,347	4834,431	2891,827
10	2647,834	5001,219	2959,552
15	2681,769	5074,579	2997,859
20	2701,397	5319,229	3027,625

As summarized in **Table III.5**, all calculated acoustic velocities (v_l, v_t, v_m) and the exhibit a continuous and steady increase with hydrostatic pressure up to **20GPa**. This upward trend directly indicates that the high-pressure stiffening of the mechanical moduli (B, G) completely

overcomes the crystalline density (ρ) expansion. Consequently, this numerical evolution confirms that external loading significantly strengthens the interatomic chemical bonds, thereby enhancing the global structural rigidity and thermal stability of the SrSe crystal matrix.

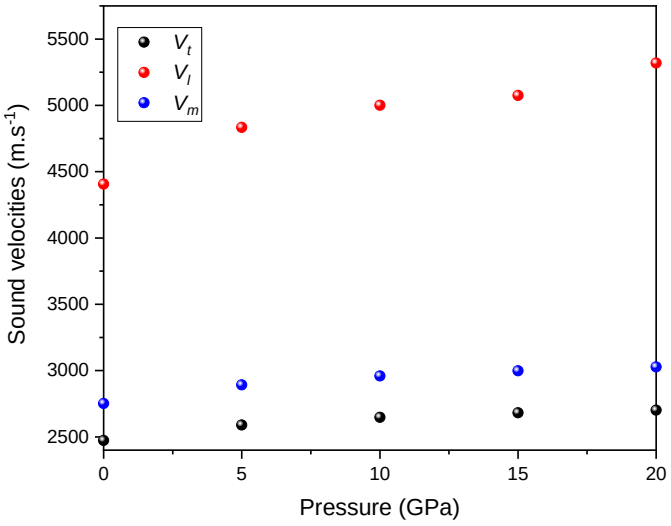


Figure III. 6: Variation of sound velocities of SrSe compound function of pressure

As illustrated in **Figure III.6**, all three acoustic velocity components (v_l, v_t and v_m) exhibit a monotonic and continuous upward trend as the hydrostatic pressure rises from **0GPa** to **20GPa**. This acceleration is governed by the rapid pressure-induced stiffening of the mechanical moduli (B and G), which overcompensates for the simultaneous increase in the crystalline density (ρ) Furthermore, the longitudinal velocity (v_l) remains significantly higher than the transverse velocity (v_t) because longitudinal waves directly encounter the strong electrostatic resistance of the principal chemical bonds during volume compression.

The thermodynamic Debye temperature **(θ_D)** follows a similar continuous upward scaling under compression, as plotted in **Figure III.7**. In solid-state physics, **θ_D** is a fundamental indicator of lattice vibrational frequencies and chemical bond strength. This steady enhancement demonstrates that high hydrostatic pressure forces a significant contraction of the unit cell, which stiffens the interatomic acoustic vibrations (phonons) and enhances the global thermal stability and structural compactness of the SrSe compound.

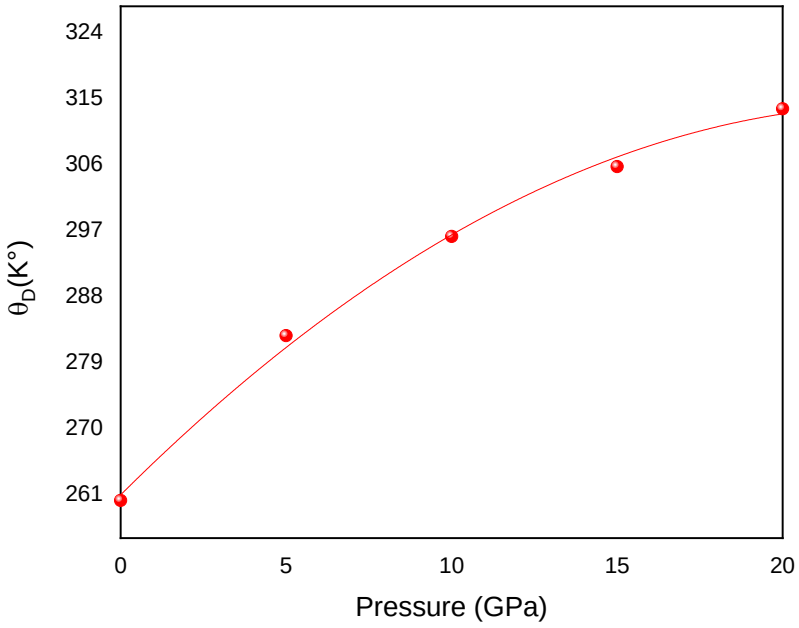


Figure III. 7 Debye temperature of the studied SrSe.

III.5 Electronic Properties

III.5.1 Energy Band Structures under Pressure

To systematically explore the electronic characteristics of the SrSe crystal, the fundamental energy band structures were processed along the high-symmetry directions of the first Brillouin zone under distinct hydrostatic pressures **(0GPa to 15GPa)**, as illustrated in **Figure III.8**.

At ambient ground-state conditions **(P = 0GPa),** the valence band maximum (VBM) and the conduction band minimum (CBM) are both precisely localized at the high-symmetry Γ-point. This electronic positioning rigorously confirms that SrSe is a semiconductor with an indirect energy band gap **(Eg).** As the hydrostatic loading scales up to **15GPa**, the energy bands display a dynamic shifting behaviour but do not close or overlap, demonstrating that the periodic crystal strictly maintains its semiconducting phase under high load environments.

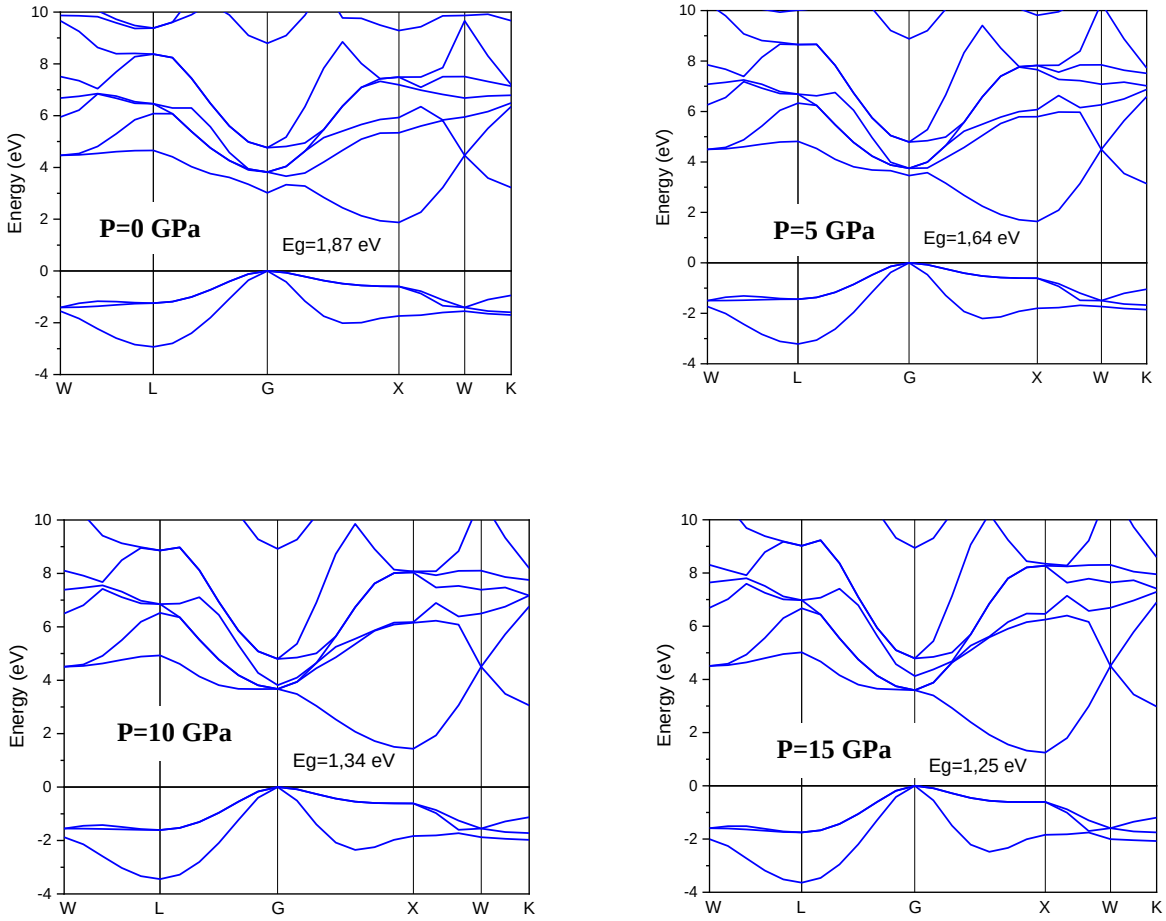


Figure III. 8 Band structures of SrSe at different pressures

III.5.2 Pressure Dependence of the Energy Band Gap

The progressive variation of the direct energy band gap (Eg) induced by external loading is detailed numerically in Table III.6 and illustrated graphically in Figure III.9.

Table III. 6 Pressure evolution of the calculated direct energy band gap Eg (in eV) for SrSe compound.

	Eg (eV)
P= 0GPa	2,261
P= 5GPa	2,035
P= 10GPa	1,836
P= 15GPa	1,654

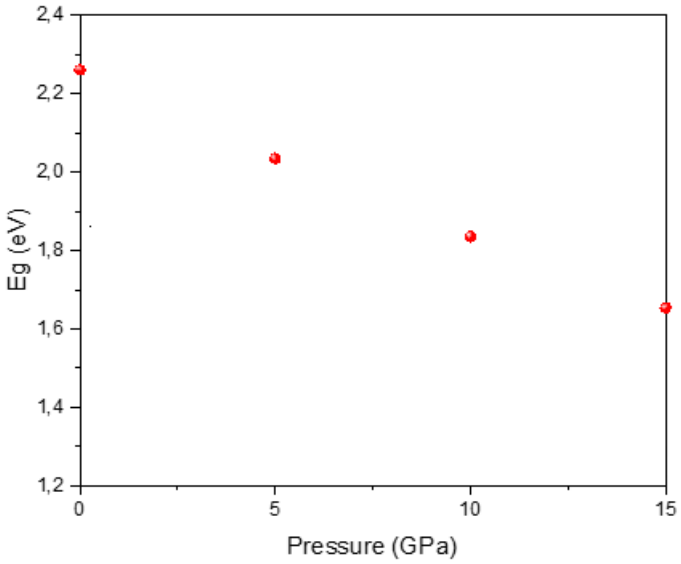


Figure III. 9 Variation of SrSe band gap with pressure

Analysis of the datasets indicates that Eg undergoes a linear and continuous narrowing behaviour as hydrostatic compression increases. The direct energy band gap drops from 2.26eV at 0GPa to 1.65 eV at 15GPa. This pressure-induced band gap narrowing is a direct physical consequence of structural contraction; the shortening of interatomic distances drastically increases atomic orbital overlapping, which broadens the energy bands and forces the conduction band edge states to shift downward toward the valence state levels.

III.5.3 Density of States (DOS) Analysis

To thoroughly understand the physical and orbital origins shaping the electronic bands, the calculated Total Density of States (TDOS) alongside the Partial Density of States (PDOS) for the SrSe matrix are displayed in **Figure III.10**

As illustrated in **Figures III.9 and III.10**, the calculated direct energy band gap (Eg) exhibits a linear and continuous narrowing behaviour as pressure rises up to 15GPa, which is a direct consequence of structural volume contraction and enhanced interatomic orbital overlapping. The corresponding density of states (DOS) spectrum clarifies that the upper valence bands near the Fermi level are predominantly governed by the Selenium (p) orbitals, whereas the lower conduction bands are derived from the unoccupied Strontium (d) states. This continuous pressure-induced band gap narrowing, driven by the strong hybridization of **Se-p** and **Sr-d** orbitals, confirms that external loading promotes a significant redistribution of electronic states and enhances the ionic-covalent bonding nature within the SrSe crystal matrix.

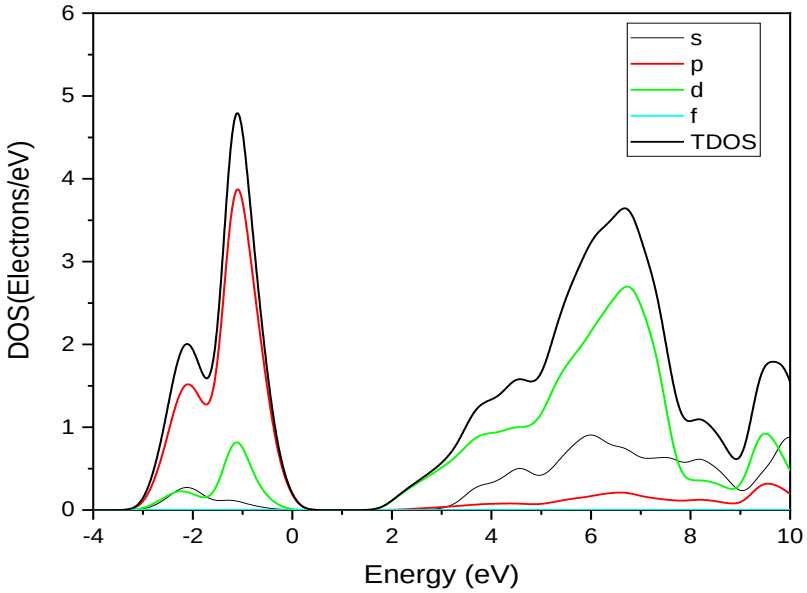


Figure III. 10 : Density of States of SrSe compound.

III.6 Conclusion

In this chapter, a comprehensive first-principles investigation was successfully conducted to evaluate the structural, mechanical, thermodynamic, and electronic properties of the cubic SrSe compound under hydrostatic pressures up to 20 GPa. The computed ground-state structural parameters show an excellent agreement with the available experimental and theoretical literature data.

The mechanical stability analysis demonstrates that while the crystal framework exhibits a continuous pressure-induced stiffening, the parameter G' drops below zero around 16 GPa, indicating a tendency toward mechanical instability at high pressure. Concurrently, the synchronized increase in the acoustic wave velocities and Debye temperature (θD) confirms the enhanced interatomic bond strength and thermal stability under high load.

Furthermore, the electronic band structure analysis reveals that SrSe is a direct semiconductor at ambient conditions of pressure and temperature. Under high compression, the strong hybridization between the Se-p and Sr-d orbitals induces a linear narrowing of the energy band gap. The band gap decreases significantly under pressure while the compound maintains its semiconducting character throughout the investigated pressure range.

References

[1] S. J. Clark et al, "First principles methods using CASTEP," *Zeitschrift für Kristallographie-Crystalline Materials*, vol. 220, no. 5-6, pp. 567-570, 2005.

[2] D. M. Ceperley and B. J. Alder, "Ground state of the electron gas by a stochastic method," *Physical Review Letters*, vol. 45, no. 7, p. 566, 1980.

[3] J. P. Perdew, K. Burke, and M. Ernzerhof, "Generalized gradient approximation made simple," *Physical Review Letters*, vol. 77, no. 18, p. 3865, 1996.

[4] R. Khenata et al, "Elastic, electronic and thermodynamic properties of SrS, SrSe and SrTe under pressure," *Computational Materials Science*, vol. 38, no. 1, pp. 29-38, 2006.

[5] M. A. Blanco, E. Francisco, and V. Luaña, "GIBBS: isothermal-isobaric thermodynamics of solids from energy curves," *Computer Physics Communications*, vol. 158, no. 1, pp. 57-72, 2004.

[6] Boudissa, R. et al. Mika Sillanpää. Prediction study of structural, electronic and optical properties of 4C16H10Br2O2 Bis (m-bromobenzoyl) methane crystals. *Biochem. Biophys. Rep.* 37, 101601. https://doi.org/10.1016/j.bbrep.2023.101601 (2024).

[7] D. Vanderbilt, Soft self-consistent pseudopotentials in generalized eigenvalue formalism, *Phys. Rev. B* 41 (1990) 7892, https://doi.org/10.1103/PhysRevB.41.7892.

[8] H.J. Monkhorst, J.D. Pack, Special points for Brillouin-zone integrations, *Phys. Rev. B* 13 (1976) 5188, https://doi. org/10.1103/PhysRevB.13.5188.

[9] SpringerMaterials, SrSe (Franzen, 1976, Fm-3m) Crystal Structure. SpringerMaterials Database. https://materials.springer.com/isp/crystallographic/docs/sd_1900389, 2026.

[10] F. D. Murnaghan, *Proceedings of the National Academy of Sciences*, vol. 30, p. 244, 1944.

[11] A. Zupan et al, *Physical Review B*, vol. 56, p. 8719, 1997.

[12] C. Kittel, *Introduction to Solid State Physics*, 8th ed. New York, NY, USA: John Wiley & Sons, 2005.

[13] P. I. Lindan and M. J. Gillan, "Shell-model potentials for strontium selenide from ab initio calculations," *Journal of Physics: Condensed Matter*, vol. 5, no. 7, pp. 1011–1022, 1993.

[14] J. F. Nye, "*Physical Properties of Crystals"*, Oxford, 1985.

[15] M. Born and K. Huang, "Dynamical Theory of Crystal Lattices", Oxford, 1954.

[16] R. Hill, *Proceedings of the Physical Society. Section A*, vol. 65, p. 349, 1952.

[17] C. Kittel, *Introduction to Solid State Physics*, 8th ed., Wiley, 2005.

[18] O. L. Anderson, *Journal of Physics and Chemistry of Solids*, vol. 24, p. 909, 1963.

General Conclusion

General conclusion

In this thesis we have studied some structural, mechanical and electronic properties of the SrSe compound.

We have primarily given the general basics about semiconductors, after that in the second chapter, it is given the theoretical part of the first principle, we investigated the DFT theory and the well-known approximations to the exchange-correlation potential: LDA and GGA. In the end of the chapter, we have presented the Castep code.

In the last chapter, we have presented the computational details and methods, the main results given that:

A good agreement of the structural parameters using BFGS approximation or by fitted E-V datas. This confirms the well-chosen parameters of calculation.

The evolution of pressure decreases the volume, and therefore the crystalline density increases gradually.

The elastic constants and the bulk modulus increase gradually with pressure but C_{11} is most important.

At 0 GPa the SrSe compound consistently maintains a brittle behaviour, which is confirmed by Cauchy pressure or Paugh's ratio.

By studying the mechanical stability criterion, we have marqued a possible phase transition at 16GPa.

This work needs to develop furthermore, by comparison with other results especially experimental ones, and it's important to do other calculations like including temperature effects and calculation of dynamical and optical properties.